Dynamics of a magnetic particle in an oscillating magnetic field

I. Misra and V. Kumaran*
Department of Chemical Engineering, Indian Institute of Science, Bangalore 560 012, India

(Received 6 February 2024; accepted 20 June 2024; published 26 July 2024)

The orientation dynamics of and the torque fluctuations due to a spheroidal magnetic particle in an oscillating magnetic field are analyzed in the Stokes flow regime. For a permanent dipole, the dynamics depends on $\omega^\dagger$, the ratio of the magnetic field frequency, and the viscous relaxation rate. For $\omega^\dagger \gg 1$, the particle executes oscillations with amplitude $\sim(\omega^\dagger)^{-1}$ about its initial orientation. The average torque is zero because the particle does not execute complete rotations, and the root mean square of the torque fluctuations scaled by the characteristic magnetic torque tends to a constant in this limit. For $\omega^\dagger \ll 1$, the orientation is close to the magnetic field direction for most of the oscillation period, and it rapidly rotates when the field passes through extrema. The scaled root mean square of the torque fluctuations is proportional to $(\omega^\dagger)^{-1/2}$ in this limit. The particle orientation aligns along the magnetic field direction for different models of induced dipoles if the magnetization is nonhysteretic. For the hysteretic Stoner-Wohlfarth model, the dynamics also depends on the parameter h_0, the ratio of the Zeeman energy, and the anisotropy energy. For $h_0 \ll 1$, the magnetic moment oscillates about one pole of the orientation vector, and the orientation vector rapidly rotates when the field passes through extrema in a manner similar to that for a permanent dipole. For $h_0 \gg 1$, the magnetic moment switches between the two poles of the orientation vector, and the orientation vector executes small amplitude oscillations about the field direction. There is a discontinuous transition between the oscillating and switching magnetic moment which depends on h_0 and the initial orientation.

DOI: 10.1103/PhysRevFluids.9.074303

I. INTRODUCTION

Suspensions of magnetic particles subjected to external magnetic fields have been used to enhance mixing and transport in microfluidic applications [1]. Due to the small dimensions, low velocities, and consequently the low Reynolds number, mixing between fluid streams occurs due to molecular diffusion in the absence of external forcing. Molecular diffusion is a slow process, and mixing due to molecular diffusion acts as a significant technological barrier for realizing the potential of microfluidics [2,3]. This is because the molecular diffusion coefficient is $10^{-9}\,\mathrm{m}^2/\mathrm{s}$ for small molecules and could be as small as $10^{-13}\,\mathrm{m}^2/\mathrm{s}$ for large molecules such as proteins and polymers. From dimensional analysis, for diffusion across a distance 1 mm, the characteristic diffusion time is in the range 10^3–10^7 s. This long mixing time makes fluid-handling operations infeasible in point-of-care devices, and it is necessary to enhance mixing by passive or active means. One of the phenomena used to enhance mixing is the application of time and spatially varying magnetic fields, which induce forces and torques in magnetic particles [4]. Active mixing strategies include magnetic microstirrer arrays [5], which rotate under an externally applied rotating magnetic field. Microconvection has been observed in suspensions of magnetic particles under spatially varying [6] and temporally oscillating [7] magnetic fields.

*Contact author: kumaran@iisc.ac.in

Magnetic particles are classified into two types, nanometer-sized particles used in ferrofluids [8], and micrometer-sized particles using in magnetorheological applications. Ferrofluids are dense colloidal suspensions where Brownian motion is important. The particles in a ferrofluid exert a torque on the fluid under the influence of a magnetic field, and this torque results in an antisymmetric part of the rate of deformation tensor [9,10] which could induce secondary flows. Issues of importance in ferrofluids are the "spin viscosity" in the momentum conservation equation [11] and spin-up flows under rotating magnetic fields [12]. Dilute ferrofluid suspensions have been used to generate mixing in microfluidic devices [13,14].

Suspensions of micrometer-sized particles are classified as magnetorheological fluids [15,16]. These are non-Brownian suspensions which flow like a Newtonian fluid in the absence of a magnetic field. Under the effect of an applied magnetic field, the particles aggregate, jam the conduit, and prevent flow. Due to the rapid jamming under a field within time intervals of the order of milliseconds, these fluids enable rapid switching of mechanical characteristics in brakes and dampers. In these dense suspensions, particle magnetic and hydrodynamic interactions play an important role in the aggregation of particles and jamming of the suspension [17]. The rheology of these fluids has usually been characterized using the "yield stress" formalism [18], but recent studies suggest that the phenomenon is more complex involving hydrodynamic and magnetic interactions [19].

From a fundamental perspective, the simplest configuration is a single particle with a magnetic moment in a steady or time-varying magnetic field with or without shear. The dynamics of a magnetic spheroid under a steady applied magnetic field has been studied in the presence of imposed shear [20–24]. In the absence of a magnetic field, a spheroid in shear flow executes closed orbits called Jeffery orbits which depend on the initial orientation. The particles' magnetic moments align with the field direction in the absence of a shear flow. As the ratio of the magnetic to hydrodynamic torque is increased, there is a progression between these two limits through a series of bifurcations, which depend on the aspect ratio of the particle. Most studies consider a permanent dipole with a fixed magnetic moment, though simple models for a nonhysteretic induced dipole have also been considered [23,24]. However, the hysteretic nature of the magnetic moment has not been incorporated in these studies.

There have been several studies on the dynamics of a particle in a rotating magnetic field [25,26]. Rotating magnetic fields have been used to propel and direct screw-shaped magnetic particles for targeted diagnostics and drug delivery [27], and they have been used for "rotational magnetic spectroscopy" for probing rheology [28]. The single-particle dynamics of spherical particles with a permanent dipole in a rotating magnetic field has been studied analytically [29]. However, there have been relatively few studies of more realistic hysteretic and nonhysteretic models for the particle magnetic moment.

The subject of the present study is the dynamics of a particle in a spatially uniform and oscillating magnetic field in the low Reynolds number regime. Though an oscillating field is much easier to generate in comparison to a rotating field, there have been relatively few studies on the particle dynamics in an oscillating field. Since there is no spatial variation in the field, an isolated particle will not experience a force. However, there could be a torque if the particle moment is not parallel to the field direction. This torque could generate fluid velocity fluctuations, and thereby convective transport and mixing. However, to evaluate the potential for mixing, it is important to examine whether the fluctuations are self-sustaining or whether they decay with time.

The dynamics of an isolated spheroidal particle in an oscillating magnetic field is the subject of this study. An important classification of magnetic particles is into permanent and induced dipoles. Permanent dipoles have a magnetic moment even in the absence of a magnetic field and are usually made of ferromagnetic materials [30]. Induced dipoles have a magnetic moment in the presence of a magnetic field and are usually made up of paramagnetic materials. The permanent dipoles considered here have a magnetic moment vector that has a fixed magnitude and direction in the particle reference frame. Magnetic particles can also be classified as single domain and multidomain. The magnetization is uniform throughout the volume in single-domain particles [31]. The magnetic moment is the product of the particle volume and the saturation magnetization. There

is an upper limit on the size of single domain particles [32,33], which is less then 100 nm for typical magnetic materials. Particles with larger size have multiple domains which are oriented in different directions. This is due to the balance between the demagnetizing energy which tends to randomize the magnetic moment and the energy of the exchange interactions which tend to keep the moments aligned. For larger particle sizes, the demagnetising energy is dominant, and the equilibrium state has multiple domains. The magnetic particles could also be anisotropic, that is, they can be magnetized along a preferred direction [34]. This anisotropy could be due to crystalline anisotropy, due to the shape of the particles or due to elastic stresses. For particles with shape anisotropy such as spheroids, the magnetization could be preferentially along the axis of the particle.

The Stoner-Wohlfarth model is for spheroidal magnetic particles that are in the single-domain state, and that have an easy axis. Here it is also assumed that the magnetic moment responds instantaneously to changes in the magnetic field, that is, the Néel relaxation time for the magnetic moment is much smaller than viscous relaxation time for the particle or the period of oscillation of the magnetic field. The Néel relaxation time is defined as

$$\tau_N = \tau_0 \exp\left(KV/k_B T\right), \tag{1}$$

where K is the magnetic anisotropy energy density, V is the particle volume, k_B is the Boltzmann constant, T is the absolute temperature, and τ_0 is an "attempt period" (inverse of attempt frequency), which is in the range 10^{-9}–10^{-10} s [35]. The Néel relaxation time is an exponential function of the ratio of the anisotropic energy and the thermal energy. Here we are considering the low anisotropy energy or high temperature limit, where the Néel relaxation time is small, and the switching of the magnetic moment between the two directions along the easy axis is instantaneous.

The model for the magnetic moment of the particle is an important aspect considered here. Though the magnetic moment for real particles has a nonlinear and hysteretic dependence on the applied magnetic field, most models consider a constant magnetic moment. In order to evaluate the potential for microfluidic mixing, it is important to consider realistic models for the particle magnetic moment, both without and with hysteresis. Here the nonhysteretic models considered are the permanent dipole with a constant magnetic moment and three models for the induced dipole. In all nonhysteretic models, the magnetic moment is considered to be along the axis of the spheroid. In the hysteretic Stoner-Wohlfarth model, the particle moment is not aligned along the particle axis. The angle between the magnetic moment and the particle axis is determined by minimizing total energy of the system, which is the sum of the Zeeman energy and the anisotropic energy due to the misalignment of domains. All of these models are examined to determine whether there are self-sustaining fluctuations in the orientation vector and the torque exerted by the particle on the fluid.

The torque balance equation for a spheroidal particle in a magnetic field is used to determine the equation for orientation angle relative to the direction of the magnetic field in Sec. II. The different models for the particle magnetic moment are described in Sec. III, and the dimensionless parameters are discussed. The dynamics for a permanent dipole with constant magnetic moment, in Sec. IV, depends on one dimensionless group $\omega^{\dagger}$, which is the magnetic field frequency scaled by the viscous relaxation rate.

The nonhysteretic models for the induced dipoles include the signum model where the magnetic moment has a constant value directed along the component of the magnetic field along the particle axis, and the linear model, where the particle magnetic moment is a linear function of the component of the field along the particle axis. The Langevin model provides a smooth progression from the linear model at low magnetic field to a constant magnetic moment at high magnetic field. In all non-hysteretic models, a trivial solution is obtained where the particle orientation is time-independent and aligned along the magnetic field in the long-time limit. This can be shown analytically for the signum and linear models, and the same solution is obtained numerically for the Langevin model. Though the solutions are trivial, the calculations are included in Appendix for completeness.

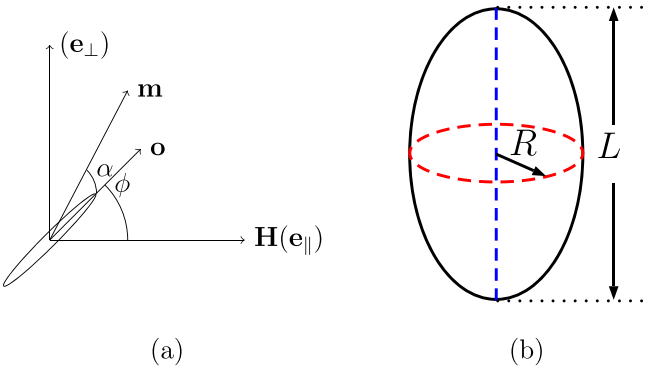

FIG. 1. The coordinate system (a) used for analyzing the dynamics of the spheroid showing the directions of the magnetic field $\boldsymbol{H}$, magnetic moment $\boldsymbol{m}$, and orientation vector $\boldsymbol{o}$ and the angles α and ϕ, and the spheroid (b) showing the axis (blue) of length L and the equatorial plane (red) of radius R.

The hysteretic Stoner-Wohlfarth model is discussed in Sec. V. The root mean squares of the torque fluctuations generated due to these different models are compared in Sec. VI, in order to estimate the relative efficiency of mixing. The important conclusions are summarized in Sec. VII.

II. EVOLUTION EQUATIONS

The effect of an oscillating magnetic field $\boldsymbol{H}$ on a spheroid with orientation vector $\boldsymbol{o}$ is studied using the coordinate system in Fig. 1(a). The spheroid is a surface of rotation of an ellipse around the axis (blue) shown in Fig. 1(b). The length of the axis is L, and the radius of the equatorial plane (red) that bisects the axis is R. The aspect ratio r is the ratio of the length along the axis and the diameter on the equatorial plane, $L/(2R)$. The spheroid is prolate for $r > 1$ and oblate for $r < 1$. The spheroid is a sphere for $r = 1$, an infinitesimal thin rod in the limit $r \gg 1$, and an infinitesimally thin disk in the limit $r \ll 1$. The magnetic field oscillates along the direction $\boldsymbol{e}_\parallel$, and $\boldsymbol{e}_\perp$ is perpendicular to $\boldsymbol{e}_\parallel$ in the $\boldsymbol{e}_\parallel - \boldsymbol{o}$ plane. The orientation vector $\boldsymbol{o}$ subtends an angle ϕ with respect to the $\boldsymbol{e}_\parallel$,

$$\boldsymbol{o} = \cos(\phi)\boldsymbol{e}_\parallel + \sin(\phi)\boldsymbol{e}_\perp. \tag{2}$$

The magnetic moment $\boldsymbol{m}$ acting on the polarizable particle due to the field makes an angle α with the orientation vector,

$$\boldsymbol{m} = m[\cos(\phi + \alpha)\boldsymbol{e}_\parallel + \sin(\phi + \alpha)\boldsymbol{e}_\perp], \tag{3}$$

where m is the magnitude of magnetic moment of the particle. The following vector products are used later in the analysis:

$$\boldsymbol{m} \cdot \boldsymbol{o} = m\cos(\alpha), \tag{4}$$

$$\boldsymbol{o} \cdot \boldsymbol{H} = H\cos(\phi), \tag{5}$$

$$\boldsymbol{m} \times \boldsymbol{H} = -mH\sin(\phi + \alpha)\boldsymbol{e}_\vdash, \tag{6}$$

$$\boldsymbol{m} \cdot \boldsymbol{H} = mH\cos(\phi + \alpha), \tag{7}$$

where H is the magnetic field, $\boldsymbol{e}_\vdash = \boldsymbol{e}_\parallel \times \boldsymbol{e}_\perp$ is the direction perpendicular to the plane of $\boldsymbol{e}_\parallel$ and $\boldsymbol{e}_\perp$ in Fig. 1.

In the viscous limit, the sum of the magnetic and hydrodynamic torques acting on the spheroid is zero. The torque balance is given by

$$A_\perp(\boldsymbol{I}-\boldsymbol{oo})\cdot\left(\tfrac{1}{2}\boldsymbol{\omega}-\boldsymbol{\Omega}\right)+A_\parallel\boldsymbol{oo}\cdot\left(\tfrac{1}{2}\boldsymbol{\omega}-\boldsymbol{\Omega}\right)+\mu_0(\boldsymbol{m}\times\boldsymbol{H})=0. \tag{8}$$

Here $\boldsymbol{\omega}$ is the fluid vorticity at the particle center in the absence of the particle, $\frac{1}{2}\boldsymbol{\omega}$ is the fluid rotation rate, $\boldsymbol{\Omega}$ is the particle angular velocity, and μ_0 is the magnetic permeability. The last term on the right in Eq. (8), $\mu_0(\boldsymbol{m}\times\boldsymbol{H})$, is the magnetic torque acting on the particle. The first two terms in Eq. (8) are the components of the hydrodynamic torque perpendicular and parallel to the orientation vector, which is along the axis of the spheroid shown in Fig. 1(b).

The coefficients $A_\parallel$ and $A_\perp$ are the ratio of the torque and the angular velocity components parallel and perpendicular to the orientation vector, respectively [36],

$$A_\parallel=\frac{16\pi\eta R^3(1+r^2)}{3(r^2\beta_\parallel+\beta_\perp)}, \tag{9}$$

$$A_\perp=\frac{16\pi\eta R^3}{3\beta_\perp}, \tag{10}$$

where η is the viscosity. The factors $\beta_\perp$ and $\beta_\parallel$ are

$$\beta_\parallel=\int_0^\infty\frac{\mathrm{d}\lambda}{(r^2+\lambda)^{3/2}(1+\lambda)},\quad \beta_\perp=\int_0^\infty\frac{\mathrm{d}\lambda}{(r^2+\lambda)^{1/2}(1+\lambda)^2}, \tag{11}$$

where λ is an integration variable.

For the special case of a spherical particle, the aspect ratio r is 1. The integrations in Eq. (11) can be carried out analytically to obtain $\beta_\parallel=\beta_\perp=\frac{2}{3}$, and we obtain the result $A_\parallel=A_\perp=8\pi\mu R^3$ for a sphere. It is necessary to determine $A_\parallel$ and $A_\perp$ numerically for other values of the aspect ratio.

The torque balance along the orientation vector is determined by taking the dot product of Eq. (8) with $\boldsymbol{o}$,

$$\boldsymbol{o}\cdot\left(\tfrac{1}{2}\boldsymbol{\omega}-\boldsymbol{\Omega}\right)=0. \tag{12}$$

Note that $\boldsymbol{o}\cdot(\boldsymbol{m}\times\boldsymbol{H})=0$ because $\boldsymbol{o}$, $\boldsymbol{m}$, and $\boldsymbol{H}$ are in the same plane. Equation (12) implies that the components of the particle angular velocity and the fluid rotation rate along the orientation vector are equal. The torque balance perpendicular to the orientation vector is obtained by taking the cross product of Eq. (8) with $\boldsymbol{o}$,

$$A_\perp\boldsymbol{o}\times\left(\tfrac{1}{2}\boldsymbol{\omega}-\boldsymbol{\Omega}\right)+\mu_0\boldsymbol{o}\times(\boldsymbol{m}\times\boldsymbol{H})=0. \tag{13}$$

The rate of change of the orientation vector is the angular velocity of the particle, $\boldsymbol{\Omega}$,

$$\begin{aligned}\frac{\mathrm{d}\boldsymbol{o}}{\mathrm{d}t}=\boldsymbol{\Omega}\times\boldsymbol{o}&=-\frac{\mu_0}{A_\perp}\boldsymbol{o}\times(\boldsymbol{m}\times\boldsymbol{H})\\&=\frac{\mu_0}{A_\perp}[(\boldsymbol{m}\cdot\boldsymbol{o})\boldsymbol{H}-(\boldsymbol{o}\cdot\boldsymbol{H})\boldsymbol{m}].\end{aligned} \tag{14}$$

Here we have used Eq. (13) for $\boldsymbol{o}\times\boldsymbol{\Omega}$, and assumed there is no flow, $\boldsymbol{\omega}=0$. The evolution equation is obtained by substituting Eqs. (2) and (3) in Eq. (14),

$$\frac{\mathrm{d}\phi}{\mathrm{d}t}=-\frac{\mu_0 mH}{A_\perp}\sin(\phi+\alpha). \tag{15}$$

For an oscillating magnetic field, $H=H_0\cos(\omega t)$, where ω is the field frequency and H_0 is the amplitude of the oscillating field. Thus, the evolution equation is

$$\frac{\mathrm{d}\phi}{\mathrm{d}t}=-\frac{\mu_0 mH_0}{A_\perp}\sin(\phi+\alpha)\cos(\omega t). \tag{16}$$

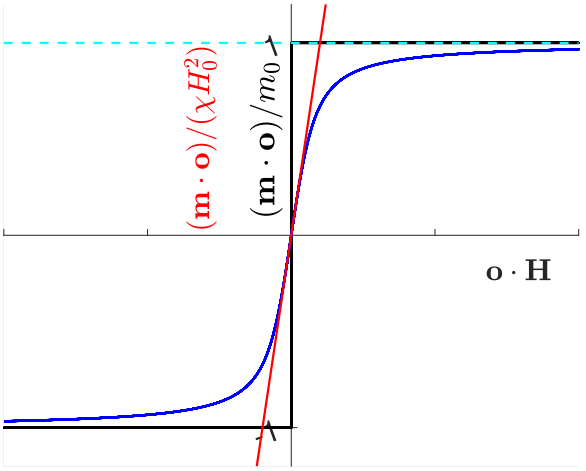

FIG. 2. The magnetic moment as a function of the component of the magnetic field along the particle axis for the nonhysteretic models: cyan—permanent dipole, black—signum model, red—linear model, blue—Langevin model.

If m_0 is the characteristic magnetic moment, it is evident from the above equation that $(A_\perp/(\mu_0 m_0 H_0))$ is a characteristic timescale, the magnetic relaxation time, which can be used to scale the time coordinate. Therefore, the scaled equations are expressed in terms of the characteristic time $t^\dagger = (t\mu_0 m_0 H_0/A_\perp)$ and the scaled frequency $\omega^\dagger = (\omega A_\perp/(\mu_0 m_0 H_0))$. It should be noted that the characteristic moment m_0 depends on the magnetization model used; the different models are discussed in Sec. III.

The torque acting on the particle is in the direction perpendicular to the magnetic field and the particle orientation [Eq. (6)],

$$\boldsymbol{T} = \mu_0(\boldsymbol{m} \times \boldsymbol{H}) = -\mu_0 m H_0 \sin(\phi + \alpha)\cos(\omega^\dagger t^\dagger)\boldsymbol{e}_\vdash. \tag{17}$$

The magnitude of the torque is related to the time derivative of ϕ using Eq.(16),

$$T = A_\perp \frac{\mathrm{d}\phi}{\mathrm{d}t}. \tag{18}$$

The average torque and the root mean square of the torque fluctuation are given by

$$T_{\mathrm{avg}} = \left(\frac{\omega}{2\pi N}\int_0^{2\pi N/\omega} T\,\mathrm{d}t\right), \tag{19}$$

$$T_{\mathrm{rms}} = \left(\frac{\omega}{2\pi N}\int_0^{2\pi N/\omega} (T - T_{\mathrm{avg}})^2\mathrm{d}t\right)^{1/2}, \tag{20}$$

where N, the number of periods of the oscillating field used for averaging, is large. The average torque is nonzero only if a particle undergoes complete rotation. For an oscillating particle, the average torque is equal to zero, and results are reported here only for T_{rms}.

III. MODELS

The magnetic moment is, in general, a function of the magnitude of the magnetic field $H = H_0\cos(\omega t)$ and the angle between the orientation vector and the magnetic field ϕ. The relation between the magnetic moment and the magnetic field is shown in Figs. 2 and 4, and the parameters

TABLE I. F and α values for the different models.

Model	F	α
Permanent dipole	m_0	0
Signum	$m_0\text{sgn}[\cos(\omega t)\cos(\phi)]$	0
Linear	$\chi H_0 \cos(\omega t)\cos(\phi)$	0
Langevin	$m_0\left[\coth\left(\frac{3\chi H_0\cos(\omega t)\cos(\phi)}{m_0}\right) - \frac{m_0}{3\chi H_0\cos(\omega t)\cos(\phi)}\right]$	0
Stoner-Wohlfarth	m_0	Eqs. (26) and (27)

are described in Table I. The models for permanent and nonhysteretic induced dipoles considered here are as follows:

(1) The simplest is the permanent dipole, where the magnetic moment has constant magnitude and is directed along the particle orientation vector,

$$\boldsymbol{m} = m_0\boldsymbol{o}. \tag{21}$$

Here m_0 is the constant magnetic moment.

(2) In the signum model for an induced dipole, the magnetic moment has constant magnitude, but is always directed along the the component of the magnetic field along the orientation vector,

$$\boldsymbol{m} = m_0\text{sgn}[\boldsymbol{o}\cdot\boldsymbol{H}]\boldsymbol{o} = m_0\text{sgn}[H_0\cos(\phi)\cos(\omega t)]\boldsymbol{o}. \tag{22}$$

Therefore, the direction of the magnetic moment changes instantaneously the dot product of the magnetic field and the orientation vector changes.

(3) In the linear model, the magnetic moment is a linear function of the component of the magnetic field along the particle orientation vector, $\boldsymbol{o}\cdot\boldsymbol{H}$, that is,

$$\boldsymbol{m} = \chi(\boldsymbol{o}\cdot\boldsymbol{H})\boldsymbol{o} = \chi H_0\cos(\phi)\cos(\omega t)\boldsymbol{o}. \tag{23}$$

Here χ is the magnetic susceptibility.

(4) The magnetic moment in the Langevin model is given by

$$\boldsymbol{m} = m_0\left[\coth\left(\frac{3\chi\boldsymbol{H}\cdot\boldsymbol{o}}{m_0}\right) - \frac{m_0}{3\chi\boldsymbol{H}\cdot\boldsymbol{o}}\right]\boldsymbol{o}. \tag{24}$$

The Langevin model exhibits a transition from a linear dependence of the moment on the field at low magnetic field and a saturation of the moment at high magnetic field, as shown in Fig. 2. The signum model is an approximation for the Langevin model in the limit $\frac{m_0}{3\chi|\boldsymbol{H}|} \ll 1$, and the linear model is an approximation in the limit $\frac{m_0}{3\chi|\boldsymbol{H}|} \gg 1$.

The models discussed above have no hysteresis. In these models, the magnetic moment is aligned with the orientation vector, and the angle α is zero.

In the Stoner-Wohlfarth model, the strength of the moment remains constant, but the moment is free to rotate in the plane containing the orientation vector and the magnetic field. The magnetic moment is given by Eq. (3) with a nonzero angle α between the orientation vector and the magnetic moment. The direction of the moment is determined from energy minimization, that is, the sum of the Zeeman energy due to the external field and anisotropy energy should be minimum. The energy E of the Stoner particle is

$$E = -\mu_0\boldsymbol{m}\cdot\boldsymbol{H} + K\sin(\alpha)^2. \tag{25}$$

The Zeeman energy is the first term on the right, $-\mu_0\boldsymbol{m}\cdot\boldsymbol{H}$. The second term on the right, $K\sin(\alpha)^2$, is the anisotropic energy due to the nonalignment of the moment with the particle axis.

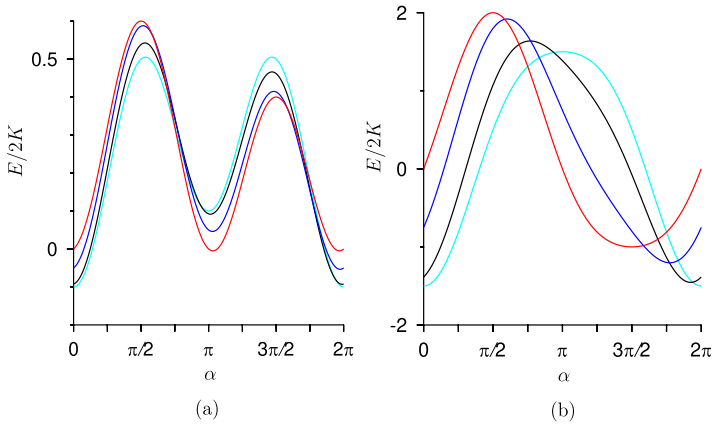

FIG. 3. The variation of the scaled energy $(E/2K)$ as a function of the angle α for different values of ϕ for the Stoner-Wohlfarth model for $\phi = \pi/2$ (red), $\phi = \pi/3$ (blue), $\phi = \pi/8$ (black), and $\phi = 0$ (cyan). Movie 1 [37] shows the variation in the energy profile for different values of ϕ for $h = 0.1$ and $h = 1.5$.

The energy E is minimum for a particular orientation of the particle when the variation of the energy with angle α is zero, and the second derivative is positive,

$$\frac{1}{2K}\frac{\partial E}{\partial \alpha} = \sin(\alpha)\cos(\alpha) + h\sin(\phi+\alpha) = 0, \tag{26}$$

$$\frac{1}{2K}\frac{\partial^2 E}{\partial \alpha^2} = \cos(2\alpha) + h\cos(\phi+\alpha) \geqslant 0. \tag{27}$$

Here $[h = \mu_0 m_0 h/(2K)]$ is the dimensionless ratio of the magnetic energy due to field to the energy of anisotropy. It should be noted that h is time-dependent, because $H = H_0\cos(\omega t)$. This is different from the constant parameter $h_0 = (\mu_0 m_0 H_0/2K)$ used in Sec. V for an oscillating magnetic field.

The energy, scaled by $2K$, is shown as a function of α for different values of ϕ in Fig. 3(a) for $h = 0.1$ and Fig. 3(b) for $h = 1.5$. For $h < 1$, the energy has two minima for two different values of α. Analytical solutions exist only for the orientations $\phi = 0$ and $\pi/2$.

(1) For $\phi = 0$, the locations of the extrema where $(\partial E/\partial\alpha) = 0$ are

$$\begin{aligned}
\alpha = 0, \quad \frac{E}{2K} = -h, \quad \frac{1}{2K}\frac{\partial^2 E}{\partial\alpha^2} = 1+h,\\
\alpha = \pi, \quad \frac{E}{2K} = h, \quad \frac{1}{2K}\frac{\partial^2 E}{\partial\alpha^2} = 1-h,\\
\cos(\alpha) = -h, \quad \frac{E}{2K} = \frac{1+h^2}{2}, \quad \frac{1}{2K}\frac{\partial^2 E}{\partial\alpha^2} = -(1-h^2).
\end{aligned} \tag{28}$$

For $h < 1$, there are two minima at $\alpha = 0$ and π, and the scaled energy at these two are $-h$ and h, respectively. For $h > 1$, there is one minimum at $\alpha = 0$, where $(E/K) = -h$.

(2) For $\phi = \pi/2$ the locations of the extrema are

$$\begin{aligned}
\alpha = \pi/2, \quad \frac{E}{2K} = h + \frac{1}{2}, \quad \frac{1}{2K}\frac{\partial^2 E}{\partial\alpha^2} = -(1+h),\\
\alpha = 3\pi/2, \quad \frac{E}{2K} = \frac{1}{2} - h, \quad \frac{1}{2K}\frac{\partial^2 E}{\partial\alpha^2} = -(1-h),\\
\sin(\alpha) = -h, \quad \frac{E}{2K} = -\frac{h^2}{2}, \quad \frac{1}{2K}\frac{\partial^2 E}{\partial\alpha^2} = 1-h^2.
\end{aligned} \tag{29}$$

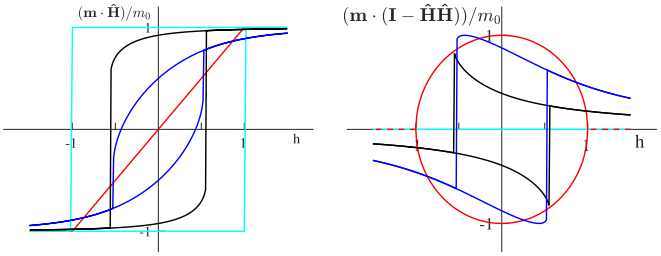

(a) (b)

FIG. 4. Component of particle moment parallel to field (a) and perpendicular to the field (b), obtained by solving Eqs. (26) and (27), for different angles between the particle and the field for the Stoner-Wohlfarth model, for $\phi = \pi/2$ (red), $\phi = \pi/3$ (blue), $\phi = \pi/8$ (black), and $\phi = 0$ (cyan).

For $h < 1$, there are two minima at $\sin(\alpha) = -h$ in the third and fourth quadrants, and the free energy is $-(h^2/2)$ at both these minima. For $h > 1$, there is one minimum at $\alpha = 3\pi/2$, where $(E/2K) = \frac{1}{2} - h$.

The values of α at the minima are obtained by numerically solving Eqs. (26) and (27) for other values of ϕ.

The solutions for α, along with the vector product given in Eq. (7), are used to determine the components of the magnetic moment parallel and perpendicular to the field. The resultant magnetization curves are shown in Figs. 4(a) and 4(b). Hysteresis is observed for values of h where there are two minima in the $(E/2K)$ vs α curves, and the moment is single-valued where there is one minimum.

The "switching field" h_s is the scaled magnetic field at which one energy minimum disappears. A particle magnetic moment with angle α located in this minimum instantaneously switches to the other energy minimum with a different α, and therefore there is a discontinuous change in the angle between the magnetic moment and the orientation vector. The switching field is a function of ϕ, the angle between orientation vector and the magnetic moment. The switching field is determined from the conditions $(\partial E/\partial\alpha) = 0$ and $(\partial^2 E/\partial\alpha^2) = 0$ [Eq. (26) and Eq. (27) with $\geqslant$ replaced by $=$]. These two conditions can be used to express h_s in terms of ϕ,

$$h_s = \frac{1}{[\sin(\phi)^{2/3} + \cos(\phi)^{2/3}]^{3/2}}. \tag{30}$$

The switching field is $h_s = 1$ for $\phi = 0$ and $\phi = \pi/2$, this is consistent with the analytical solutions (28) and (29). The switching field has a minimum value $h_s = \frac{1}{2}$ for $\phi = \pi/4$.

Since the relation between α and ϕ is given by equilibrium conditions and not time evolution equations, it is implicitly assumed that the Néel time for the response of the particle magnetic moment is small compared to the time for the change in the magnetic field or the particle orientation.

The evolution Eq. (16) can be formulated as

$$\frac{\mathrm{d}\phi}{\mathrm{d}t} = -(\mu_0 H_0/A_\perp)\cos(\omega t)\sin(\phi+\alpha)F(\phi,t), \tag{31}$$

where F is the function that relates the strength of the moment to the field. Table I gives the values of F and α for the different models analyzed in this study.

IV. PERMANENT DIPOLE

The magnetic moment is $\boldsymbol{m} = m_0\boldsymbol{o}$ [Eq. (21)], and the scaled evolution equation for this model is

$$\frac{\mathrm{d}\phi}{\mathrm{d}t^\dagger} = -\cos(\omega^\dagger t^\dagger)\sin(\phi), \tag{32}$$

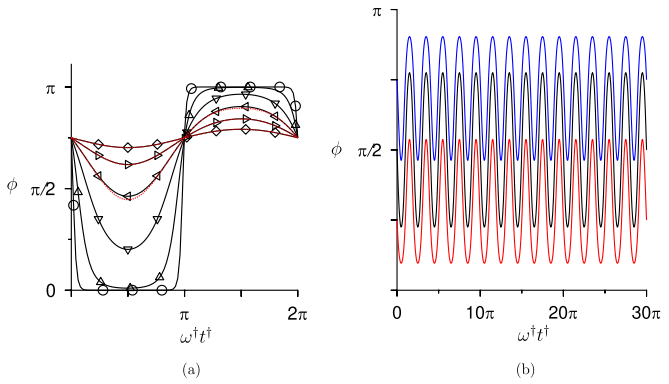

FIG. 5. The variation of the angle ϕ between the particle orientation and the magnetic field direction as a function of $\omega^\dagger t^\dagger$ for a permanent dipole for (a) $\omega^\dagger = 0.05$ ($\circ$), 0.2 ($\triangle$), 0.5 (∇), 1.0 ($\triangleleft$), 2.0 ($\triangleright$), and 5 ($\diamond$) for the initial condition $\phi_i = 3\pi/4$ at $t^\dagger = 0$, and (b) $\omega^\dagger = 1$ and $\phi_i = \pi/4$ (red), $\pi/2$ (black), and $3\pi/4$ (blue). The analytical solution [Eq. (33)] coincides with the numerical solution. The dotted red lines in (a) are the $\omega^\dagger \gg 1$ asymptotic solutions [Eq. (40)] for $\omega^\dagger = 5.0$, 2.0, and 1.0. Movie 2 [37] shows the evolution of the dynamics of the orientation vector for $\omega^\dagger = 0.05$, 0.5, and 2.0.

where the scaled time is $t^\dagger = (\mu_0 m_0 H_0 t/A_\perp)$, and the scaled frequency is $\omega^\dagger = \omega A_\perp/(\mu_0 m_0 H_0)$. The solution for Eq. (32) is

$$\cos(\phi) = \frac{A\exp[2\sin(\omega^\dagger t^\dagger)/\omega^\dagger] - 1}{A\exp[2\sin(\omega^\dagger t^\dagger)/\omega^\dagger] + 1}, \quad \sin(\phi) = \frac{2\sqrt{A}\exp[\sin(\omega^\dagger t^\dagger)/\omega^\dagger]}{A\exp[2\sin(\omega^\dagger t^\dagger)/\omega^\dagger] + 1}, \tag{33}$$

where the constant A depends on the initial condition, $\phi = \phi_i$ at $\cos(\omega^\dagger t^\dagger) = 1$,

$$A = \frac{1 + \cos(\phi_i)}{1 - \cos(\phi_i)}. \tag{34}$$

The variation of the angle ϕ with $\omega^\dagger t^\dagger$ is shown in Fig. 5(a) for different values of $\omega^\dagger$ for the same initial condition, $\phi_i = 3\pi/4$ at $t^\dagger = 0$. For $\omega^\dagger \ll 1$, the orientation is close to the two fixed points, $\phi = 0, \pi$, for most of the time, and there are rapid transitions between these two orientations. It can be inferred, as follows, that the difference $\Delta\phi$ between the angle ϕ and the fixed points is $\phi \sim 2A^{-1/2}\exp(-1/\omega^\dagger)$ near the fixed point $\phi = 0$, and $\pi - \phi \sim 2A^{1/2}\exp(-1/\omega^\dagger)$ near the fixed point $\phi = \pi$. For $\phi \ll 1$ near the fixed point at $\phi = 0$, ϕ has a minimum at $\sin(\omega^\dagger t^\dagger) = 1$. At this instant the analytical solution, Eq. (30), for $\sin(\phi)$ is

$$\sin(\phi) = \frac{2\sqrt{A}\exp(1/\omega^\dagger)}{A\exp(2/\omega^\dagger) + 1} \sim 2A^{-1/2}\exp(-1/\omega^\dagger). \tag{35}$$

Since $\sin(\phi) \simeq \phi$ for $\phi \ll 1$, we find that $\phi \sim 2A^{-1/2}\exp(-1/\omega^\dagger)$. For $\pi - \phi \ll 1$ near the fixed point at $\phi = \pi$, the maximum value of ϕ is at $\sin(\omega^\dagger t^\dagger) = -1$. At this instant, the analytical solution, Eq. (30), for $\sin(\phi)$ is

$$\sin(\phi) = \frac{2\sqrt{A}\exp(-1/\omega^\dagger)}{A\exp(-2/\omega^\dagger) + 1} \sim 2A^{1/2}\exp(-1/\omega^\dagger). \tag{36}$$

Since $\sin(\phi) \simeq \pi - \phi$ for $\pi - \phi \ll 1$, we find that $\pi - \phi \sim 2A^{1/2}\exp(-1/\omega^\dagger)$. Therefore, the orientation approaches close to the two fixed points, but it does not reach the fixed points. This is because the eigenvalues at these fixed points are time-dependent. The eigenvalue is $-\cos(\omega^\dagger t^\dagger)$ for the fixed point at $\phi = 0$, and $\cos(\omega^\dagger t^\dagger)$ for the fixed point at $\phi = \pi$. When $\cos(\omega^\dagger t^\dagger)$ is positive, $\phi = 0$ is the stable fixed point and $\phi = \pi$ is the unstable fixed point. When $\cos(\omega^\dagger t^\dagger)$ is negative,

$\phi = \pi$ is the stable fixed point and $\phi = 0$ is the unstable fixed point. Since the stability of an initially stable fixed point reverses as the orientation approaches this fixed point, the orientation never reaches the fixed point.

Figure 5(b) shows the dependence of the ϕ trajectories on the initial condition over a longer time period of 15 times the period of the magnetic field oscillation. Here ϕ is shown as a function of $\omega^\dagger t^\dagger$ for $\omega^\dagger = 1$ and for three different initial conditions, $\phi_i = \pi/4, \pi/2$, and $3\pi/4$. It is evident that the trajectories remain distinct even after tens of time periods of the magnetic field oscillation. The trajectories are in quantitative agreement with the analytical prediction, Eqs. (33) and (34).

For $\omega^\dagger \gg 1$, the response time is much larger than the period of the magnetic field oscillation. In this limit, the field direction changes before there is significant change in the orientation vector. The particle oscillates with small amplitude around the initial condition. The dynamics over one period of the magnetic field oscillation is analyzed by defining $t^\ddagger = \omega^\dagger t^\dagger$, so that the magnetic field variation is expressed as $H = H_0 \cos(t^\ddagger)$. Equation (32) is expressed in terms of $t^\ddagger$, and the resulting equation is divided by $\omega^\dagger$, to obtain

$$\frac{\mathrm{d}\phi}{\mathrm{d}t^\ddagger} = -\frac{1}{\omega^\dagger}\cos(t^\ddagger)\sin(\phi). \tag{37}$$

A regular perturbation expansion in the small parameter $(\omega^\dagger)^{-1}$, $\phi = \phi_0 + \phi_1/(\omega^\dagger) + \phi_2/(\omega^\dagger)^2 + \cdots$, of the evolution Eq. (37) gives

$$\frac{\mathrm{d}\phi_0}{\mathrm{d}t^\ddagger} = 0, \quad \frac{\mathrm{d}\phi_1}{\mathrm{d}t^\ddagger} = -\cos(t^\ddagger)\sin(\phi_0), \quad \frac{\mathrm{d}\phi_2}{\mathrm{d}t^\ddagger} = -\cos(t^\ddagger)\phi_1\cos(\phi_0). \tag{38}$$

These equations are solved sequentially with the initial condition $\phi_0 = \phi_i$, $\phi_1 = 0$ and $\phi_2 = 0$ at $t^\ddagger = 0$, to obtain

$$\phi_0 = \phi_i, \quad \phi_1 = -\sin(t^\ddagger)\sin(\phi_0), \quad \phi_2 = \tfrac{1}{2}\cos(\phi_0)\sin(\phi_0)\sin(t^\ddagger)^2. \tag{39}$$

Therefore, the expansion for the angle ϕ expressed in terms of ϕ_i and $t^\dagger$ is

$$\phi = \phi_i - (\omega^\dagger)^{-1}\sin(\omega^\dagger t^\dagger)\sin(\phi_i) + \tfrac{1}{2}(\omega^\dagger)^{-2}\cos(\phi_i)\sin(\phi_i)\sin(\omega^\dagger t^\dagger)^2. \tag{40}$$

The asymptotic solution (40) in the limit $\omega^\dagger \gg 1$ is shown by the red dotted lines for $\omega^\dagger = 5$, 2, and 1 in Fig. 5(a). The asymptotic results are in quantitative agreement with the numerical results for $\omega^\dagger \geqslant 2$, and there is very little difference between the two even at $\omega^\dagger = 1$. It is noteworthy that the asymmetry in the trajectories about $\phi = \phi_i$ is well captured by the asymptotic solution, Eq. (40), at $\omega^\dagger = 1$.

The magnitude of the torque acting on the particle, Eq. (17), is

$$T = -\mu_0 m_0 H_0 \sin(\phi)\cos(\omega^\dagger t^\dagger). \tag{41}$$

The average torque acting on the particle is zero as the particle oscillates about its initial condition and does not undergo a complete rotation. The root mean square of the torque fluctuations in the direction perpendicular to the $\boldsymbol{e}_\parallel - \boldsymbol{e}_\perp$ plane is

$$T^\dagger_{\mathrm{rms}} = \frac{T_{\mathrm{rms}}}{\mu_0 m_0 H_0} = \left(\frac{\omega^\dagger}{2\pi}\int_0^{2\pi/\omega^\dagger} \mathrm{d}t^\dagger \frac{4A\cos(\omega^\dagger t^\dagger)^2 \exp[2\sin(\omega^\dagger t^\dagger)/\omega^\dagger]}{\{A\exp[2\sin(\omega^\dagger t^\dagger)/\omega^\dagger] + 1\}^2}\right)^{1/2}. \tag{42}$$

The scaled root mean square of the torque fluctuation is plotted as a function of $\omega^\dagger$ in Fig. 6. This increases as $\sqrt{2\omega^\dagger/\pi}$ for $\omega^\dagger \lesssim 0.5$. In the limit $\omega^\dagger \gg 1$, the leading-order term in the solution (40), $\phi = \phi_i$, can be used to obtain the root mean square of the torque fluctuation,

$$T^\dagger_{\mathrm{rms}} = \frac{|\sin(\phi_i)|}{\sqrt{2}}, \tag{43}$$

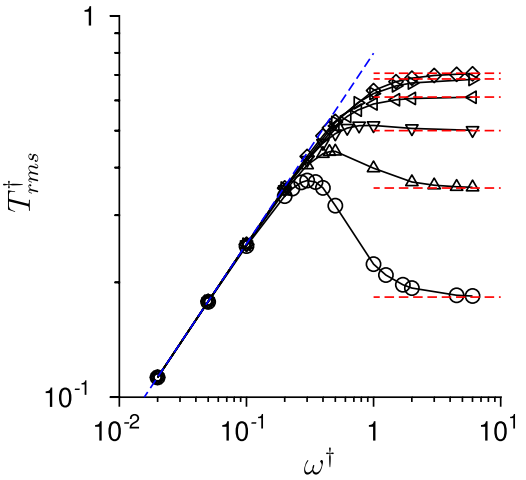

FIG. 6. The variation of root mean square of the torque fluctuation with $\omega^{\dagger}$ for a permanent dipole for initial conditions, $\phi_i = \pi/12$ ($\circ$), $\phi_i = \pi/6$ ($\triangle$), $\phi_i = \pi/4$ (∇), $\phi_i = \pi/3$ ($\triangleleft$), $\phi_i = 5\pi/12$ ($\triangleright$), and $\phi_i = \pi/2$ ($\diamond$). The blue dashed line is the asymptotic result for $\omega^{\dagger} \ll 1$, $T^{\dagger}_{\text{rms}} = \sqrt{2\omega^{\dagger}/\pi}$. The red dashed lines on the right are the asymptotic results for $\omega^{\dagger} \gg 1$ [Eq. (43)].

where ϕ_i is the initial orientation angle. The root mean square of the torque fluctuation does depend on the initial orientation for $\omega^{\dagger} \gg 1$, and the numerical results are in agreement with the high $\omega^{\dagger}$ prediction for $\omega^{\dagger} \gtrsim 5$.

V. STONER-WOHLFARTH MODEL

The scaled evolution equation for the Stoner-Wohlfarth model is

$$\frac{\mathrm{d}\phi}{\mathrm{d}t^{\dagger}} = -\sin(\phi + \alpha)\cos(\omega^{\dagger}t^{\dagger}). \tag{44}$$

The transformed energy equations (26) and (27) for an oscillating field are

$$\sin(\alpha)\cos(\alpha) + h_0\cos(\omega^{\dagger}t^{\dagger})\sin(\phi + \alpha) = 0, \tag{45}$$

$$\cos(2\alpha) + h_0\cos(\omega^{\dagger}t^{\dagger})\cos(\phi + \alpha) \geqslant 0, \tag{46}$$

where $h_0 = (\mu_0 m_0 H_0/2K)$. For a given initial orientation, the α value is determined by using the energy equations (45) and (46).

A unique feature of the Stoner-Wohlfarth model is synchronization with magnetic field, which will be discussed in detail in Secs. V A and V B. In Fig. 5(b) it was observed that the solution (33) for the orientation of a permanent dipole depends on the initial condition. In contrast, the analysis in this section shows that the periodic state in the long time limit for the Stoner-Wohlfarth model does not depend on the initial orientation. There are transients at initial time that depend on the initial orientation, but these decay with time. In the long-time limit, there is synchronization of the orientation with the magnetic field oscillation. The discussion in the following sections is restricted to the synchronized trajectories in the long-time limit.

A. Low h_0

Shown in Figs. 7(a) and 7(c) are the angles ϕ of the orientation vector (black) and $(\phi + \alpha)$ of the magnetic moment (blue), and in Fig. 7(b) and 7(d) are the angles α between the magnetic moment and the orientation vector scaled by h_0, for two different values, $h_0 = 0.1$ and $h_0 = 0.5$. Results

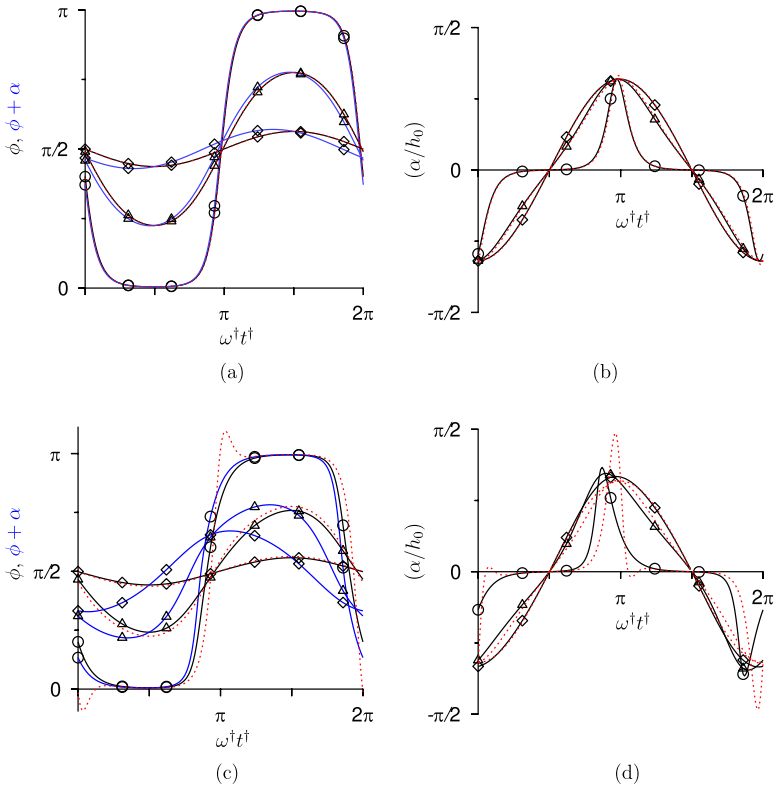

FIG. 7. The angles ϕ of the orientation vector (black), $\phi+\alpha$ of the magnetic moment (blue) in (a) and (c), and (α/h_0) in (b) and (d), as a function of $\omega^\dagger t^\dagger$ for $h_0 = 0.1$ (a) and $h_0 = 0.5$ (b), and $\omega^\dagger = 0.2(\circ)$, $\omega^\dagger = 1$ $(\triangle)$, and $\omega^\dagger = 5$ $(\diamond)$. The red dotted lines in (a) and (c) are the solutions $\phi_0 + h_0\phi_1$, where ϕ_0 is the solution for permanent dipole [Eqs. (33) and (34)] with $\phi_i = \pi/2$, and ϕ_1 is the first correction [Eq. (49)]. The red dotted lines in (b) and (d) are the first approximation α_1 [Eq. (47)]. Movies 3 and 4 [37] show the dynamics of the orientation and magnetic moment vectors for $h_0 = 0.1$ and 0.5, respectively.

are provided for three different values of $\omega^\dagger$, 0.2, 1, and 5. For $h_0 = 0.1$ [Figs. 7(a) and 7(b)], the trajectories are qualitatively similar to those for a permanent dipole shown in Fig. 5, and the angle α is small. [Note that the ratio $(\alpha/h_0) = 10\alpha$ is plotted in Fig. 7(b).] For $\omega^\dagger = 0.2$, the time period of the magnetic field is much larger than the orientation relaxation time. The orientation vector and moment are aligned with the magnetic field direction $(\phi = 0, \pi)$ for most of the oscillation period, and there are sharp but continuous changes when the magnetic field passes through extrema. The magnetic moment and the orientation vector are aligned and $\alpha \approx 0$ for most of the oscillation period, and α is nonzero only when the orientation reverses. For $\omega^\dagger = 5$, when the time period of the magnetic field is much smaller than the orientation relaxation time, the amplitude of the oscillations is small and the oscillations are sinusoidal. The angle α is also sinusoidal in this case. For $\omega^\dagger = 1$, the oscillations are approximately sinusoidal, but the oscillation amplitude is larger. In all cases, the orientation angle and the magnetic moment are nearly aligned for $h_0 = 0.1$. This is designated "oscillating magnetic moment," since the magnetic moment oscillates close to one pole of the orientation vector.

There is a larger variation in the angle α between the orientation and the magnetic moment for $h_0 = 0.5$, as shown in Fig. 7(b). However, the ratio (α/h_0) is approximately the same as that for $h_0 = 0.1$. The forms of the trajectories for $h_0 = 0.5$ are qualitatively similar to those for $h_0 = 0.1$—the variation is approximately sinusoidal for $\omega^\dagger = 5$ and 1, and there is a sharp transition when the magnetic field reverses for $\omega^\dagger = 0.2$.

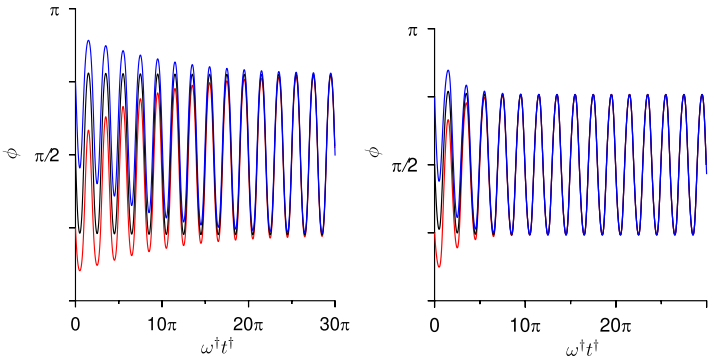

FIG. 8. The orientation angle ϕ as a function of $\omega^\dagger t^\dagger$ at $\omega^\dagger = 1$ for the Stoner-Wohlfarth model with $h_0 = 0.1$ (a), and the Stoner-Wohlfarth model with $h_0 = 0.5$ (b). The blue, black, and red lines are the trajectories for initial condition $\phi_i = 3\pi/4$, $\phi_i = \pi/2$, and $\phi_i = \pi/4$ at $t^\dagger = 0$, respectively.

It is observed that the angle α is positive when ϕ increases, and negative when ϕ decreases, indicating that the magnetic moment vector leads the orientation vector. The variation of α is smooth, and hysteresis is not observed. In the limit $h_0 \ll 1$, α is expected to be $O(h_0)$, and an expansion $\phi = \phi_0 + h_0\phi_1 + \cdots$ and $\alpha = h_0\alpha_1 + \cdots$ is employed. Since α is $O(h_0)$, it does not appear in the evolution equation for ϕ_0 obtained by expanding Eq. (44) in the limit $h_0 \ll 1$. The resulting equation reduces to that for a permanent dipole, Eq. (32), with ϕ replaced by ϕ_0. Equation (33) is the solution for ϕ_0. The leading-order contribution α_1 is then determined from Eq. (45),

$$\alpha_1 = -\cos(\omega^\dagger t^\dagger)\sin(\phi_0). \tag{47}$$

This solution, shown by the dotted red lines superposed on the black lines in Fig. 7(b), is in excellent agreement with the numerical solutions for $h_0 = 0.1$. The agreement is not as good for $h_0 = 0.5$ [Fig. 7(d)], but the qualitative variation is captured. The equation for the first correction ϕ_1 is

$$\begin{aligned}\frac{d\phi_1}{dt^\dagger} &= -(\phi_1 + \alpha_1)\cos(\phi_0)\cos(\omega^\dagger t^\dagger) \\ &= -\phi_1\cos(\phi_0)\cos(\omega^\dagger t^\dagger) + \sin(\phi_0)\cos(\phi_0)\cos(\omega^\dagger t^\dagger)^2.\end{aligned} \tag{48}$$

An important difference between the trajectories for the orientation vector for a permanent dipole in Fig. 5 and those for the Stoner-Wohlfarth model for $h_0 \ll 1$ in Fig. 7 is the dependence on initial condition. Whereas the trajectories in Fig. 5 for a permanent dipole do depend on the initial orientation, those for the Stoner-Wohlfarth model in Fig. 7 do not depend on the initial orientation. In the long-time limit, the trajectories drift to a universal trajectory that is independent of the initial angle. This phenomenon is shown in Fig. 8, where the variation of ϕ with $\omega^\dagger t^\dagger$ is shown for $h_0 = 0.1$ [Fig. 8(a)] and $h_0 = 0.5$ [Fig. 8(b)]. Here it is clear that ϕ tends to a universal trajectory in the long-time limit. To specify the universal trajectory, the angle ϕ_u is defined as the value of ϕ at the instant $\cos(\omega^\dagger t^\dagger) = 1$. In Fig. 8 it is observed that ϕ_u is close to $(\pi/2)$, independent of the initial condition. This is in contrast to the trajectory for the permanent dipole model in Fig. 5(b), where the variation of ϕ clearly depends on the initial condition.

The drift to a universal trajectory can be rationalized from the equation for the first correction ϕ_1 for the orientation angle (Eq. (48)). When the leading-order solutions, Eq. (33) for $\cos(\phi_0)$ and $\sin(\phi_0)$, are substituted into Eq. (48), the second inhomogeneous forcing term on the right is secular and does not average to zero over one cycle unless $\phi_i = \pi/2$ at $\cos(\omega^\dagger t^\dagger) = 1$. A bounded solution is obtained in the long-time limit only if there is synchronization with the applied field such that

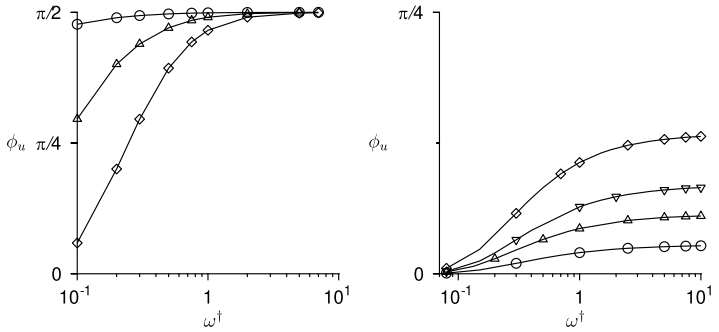

FIG. 9. The angles $\phi = \phi_u$ at $\cos(\omega^\dagger t^\dagger) = 1$ as a function of $\omega^\dagger$ for (a) an oscillating magnetic moment for $h_0 = 0.01(\circ)$, $h_0 = 0.1$ ($\triangle$), and $h_0 = 0.5$ ($\diamond$), and (b) a switching magnetic moment for $h_0 = 1.0$ ($\circ$), $h_0 = 0.8$ ($\triangle$), $h_0 = 0.7$ (∇), $h_0 = 0.6$ ($\diamond$).

$\phi_i = \pi/2$ at $\cos(\omega^\dagger t^\dagger) = 1$ in Eqs. (33) and (34). This synchronization can be understood as the consequence of two coupled oscillators in the Stoner-Wohlfarth model, one between the field and the magnetic moment and the other between the magnetic moment and the orientation vector. In contrast, there is only one oscillator in the permanent dipole model coupled to the external field, and therefore there is no synchronization.

This first-order inhomogeneous equation for ϕ_1 can be solved using an integrating factor after substituting the solutions (33) for $\cos(\phi_0)$ and $\sin(\phi_0)$,

$$\phi_1\{A\exp[2\sin(\omega^\dagger t^\dagger)/\omega^\dagger] + 1\}\exp[-\sin(\omega^\dagger t^\dagger)/\omega^\dagger]$$
$$= \int_0^{t^\dagger} \mathrm{d}t^\ddagger \left(\frac{2\sqrt{A}\{A\exp[2\sin(\omega^\dagger t^\ddagger)/\omega^\dagger] + 1\}\cos(\omega^\dagger t^\ddagger)^2}{\{A\exp[2\sin(\omega^\dagger t^\ddagger)/\omega^\dagger] + 1\}} \right) + C, \tag{49}$$

where C is the constant of integration and $t^\ddagger$ is the integration variable. The value of C is obtained from the requirement that the average of ϕ_1 is zero when the integration is carried out between $\omega^\dagger t^\dagger = 0$ and $\omega^\dagger t^\dagger = 2\pi$. The dotted red lines superposed on the black lines in Fig. 7 are the solutions for $\phi_0 + h_0\phi_1$ in the limit $h_0 \ll 1$. These are in excellent agreement for $h_0 = 0.1$, but there are differences during the rotation of the orientation vector for $h_0 = 0.5$.

As explained earlier, the universal trajectory is characterized by the parameter ϕ_u is defined as the angle ϕ at $\cos(\omega^\dagger t^\dagger) = 1$. From Fig. 7, it is observed that ϕ_u is close to $\pi/2$ for $h_0 = 0.1$, but the asymptotic result is not accurate for $h_0 = 0.5$. The variation of ϕ_u with $\omega^\dagger$ for different values of h_0 is shown in Fig. 9(a). This figure shows that ϕ_u is close to $\pi/2$ for $h_0 = 0.01$, and ϕ_u also tends to $\pi/2$ for $\omega^\dagger \gg 1$. Note that the period of the magnetic field oscillation is small compared to the particle relaxation time in the limit $\omega^\dagger \gg 1$, and the amplitude of the oscillations decreases proportional to $(\omega^\dagger)^{-1}$.

B. High h_0

Figure 10 shows the evolution of the angles [Fig. 10(a)] ϕ, and [Fig. 10(b)] α (black) and $(\phi + \alpha)$ (blue) as a function of $\omega^\dagger t^\dagger$. The difference between the range of the ordinate in Figs. 10(a) and 10(b) is noteworthy. In Fig. 10(b), the angle α varies in the range $-\pi$ to π, while the angle ϕ is positive and much smaller in magnitude in Fig. 10(a). Due to this, there is very little difference between α and $\alpha + \phi$. The difference does seem large over a part of the time interval because α is slightly less than π, and $\alpha + \phi$ is wrapped around and is slightly greater than $-\pi$.

The angles α and $\phi + \alpha$ undergo discontinuous transitions between 0 and $\pm\pi$. The reversal of the magnetic moment takes place a little after the reversal in the direction of the applied magnetic field.

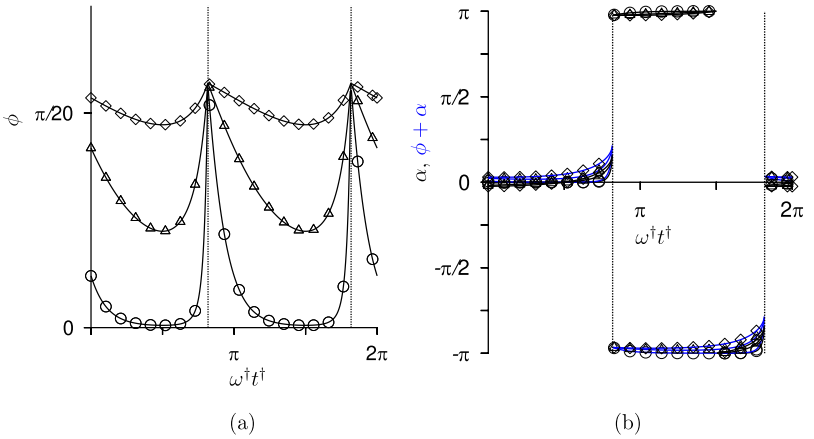

FIG. 10. The angle (a) of the orientation vector ϕ, and (b) the angles of the magnetic moment α (black) and $\phi + \alpha$ (blue) as a function of $\omega^\dagger t^\dagger$ for $h_0 = 0.8$ and $\omega^\dagger = 0.2(\circ)$, $\omega^\dagger = 1$ ($\triangle$), and $\omega^\dagger = 5$ ($\diamond$). The magnetic moment switches at the time instants shown by the vertical dotted lines. Movie 5 [37] shows the dynamics of the orientation vector and the magnetic moment for $h_0 = 0.8$ and for $\omega^\dagger = 0.2$, 1.0, and 2.0.

There is a discontinuous change because the curvature of the local minimum of the energy profile for the SW model given by (45) and (46) becomes zero, and the system transitions discontinuously to the other minimum. This is illustrated in Fig. 11, which shows the evolution of the free energy landscape for $h_0 = 0.8$ and $\omega^\dagger = 1$. In contrast to Fig. 3, the magnetic field is not a constant, but undergoes a sinusoidal oscillation $h = h_0 \cos(\omega^\dagger t^\dagger)$. Due to this, there are two minima in the free

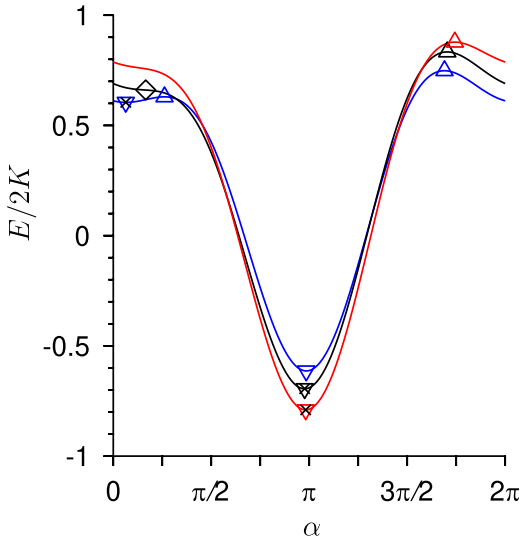

FIG. 11. The variation of the scaled energy $(E/2K)$ as a function of the angle α for the Stoner-Wohlfarth model for an oscillating field with $h_0 = 0.8$, $\omega^\dagger = 1.0$, and $\omega^\dagger t^\dagger = 2.45$, $\phi = 0.122$ (blue), $\omega^\dagger t^\dagger = 2.64$, $\phi = 0.178$ (black), and $\omega^\dagger t^\dagger = 3.27$, $\phi = 0.127$ (red). The maxima are shown by the $\triangle$ symbols, the minima by the ∇ symbols, and the inflection point with zero slope by the $\diamond$ symbol. The angle α of the particle magnetic moment and the corresponding energy are shown by the $\times$ symbol. Movie 6 [37] shows the variation of the energy profile with $\omega^\dagger t^\dagger$ for $h_0 = 0.8$ and $\omega^\dagger = 1.0$.

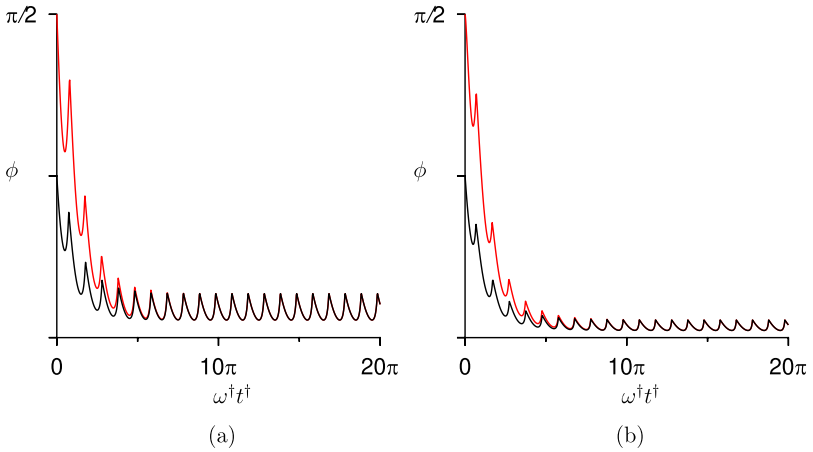

FIG. 12. The orientation angle ϕ as a function of $\omega^\dagger t^\dagger$ at $\omega^\dagger = 1$ for the Stoner-Wohlfarth model with $h_0 = 0.75$ (a), and the Stoner-Wohlfarth model with $h_0 = 1.0$ (b). The black and red lines are the trajectories for initial condition $\phi_i = \pi/4$ and $\phi_i = \pi/2$ at $t^\dagger = 0$, respectively.

energy for time intervals where $h_0 \cos(\omega^\dagger t^\dagger) < h_s$, where h_s is the switching field [Eq. (30)], and there is one minimum for time intervals where $h_0 \cos(\omega^\dagger t^\dagger) > h_s$. It should be noted that h_s is a function of ϕ, which is itself a function of time in this case. The merger of a maximum and a minimum is shown in Fig. 11(a) for $h_0 = 0.8$ and $\omega^\dagger = 1$. At $\omega^\dagger t^\dagger = 2.45$, the energy profile shown by the blue curve has two maxima and two minima. At $\omega^\dagger t^\dagger = 2.64$, shown by the black curve, there is an inflection point with zero slope due to the merger of a maximum and a minimum. At $\omega^\dagger t^\dagger = 3.27$, there is only one maximum and one minimum as shown by the red curve. Thus, there are two maxima and two minima for $\omega^\dagger t^\dagger < 2.64$, and one maximum and one minimum for $\omega^\dagger t^\dagger > 2.64$.

The α and energy values for the particle magnetic moment are shown by the $\times$ symbol in Fig. 11. For $\omega^\dagger t^\dagger = 2.45$, $\phi = 0.122$, the energy minimum is at $\alpha = 0.201$. At $\omega^\dagger t^\dagger = 2.64$, $\phi = 0.178$, the minimum merges with a maximum resulting in an inflection point at $\alpha = 0.201$, and the orientation of the magnetic moment switches (discontinuously changes) to $\alpha = 3.07$, where the other minimum is located. This transition between two minima and one minimum causes a discontinuous change in the magnetic moment along the the vertical lines in Fig. 10(b).

The ϕ trajectory in Fig. 10(a) is continuous, but there is a discontinuity in the slope along with the discontinuous change in the moment. This is because the magnetic moment discontinuity results in a discontinuous change in the torque on the particle. Due to this, the change in the angular velocity $(d\phi/dt)$ is discontinuous, and the change in ϕ is nondifferentiable. Since the magnetic moment discontinuously switches between the opposite poles of the orientation vector, this type of motion is denoted "switching magnetic moment."

The trajectories are universal, independent of the initial orientation, for the switching magnetic moment as well. The trajectories for two different initial conditions in the first quadrant are shown in Fig. 12(a) for $h_0 = 0.75$ and 12(b) for $h_0 = 1.0$. If the initial condition is in the second quadrant, the trajectories are, by symmetry, π minus the the angle shown in Fig. 12. It is clearly observed that the trajectories all converge to a universal trajectory within a few cycles of the magnetic field oscillation. As a consequence, the torque fluctuations are also independent of the initial orientation angle. The angle ϕ_u for the switching magnetic moment is shown as a function of $\omega^\dagger$ for different values of h_0 in Fig. 9(b). It is evident that ϕ_u is much smaller for a switching magnetic moment in comparison to the oscillating magnetic moment, and ϕ_u decreases as h_0 increases. This implies that the particle orientation is close to the direction of the magnetic field when the field passes through a maximum.

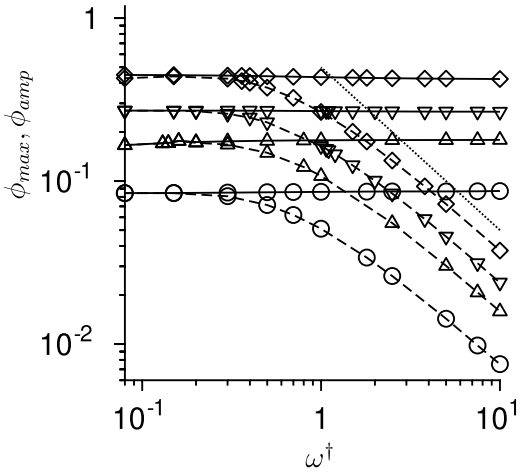

FIG. 13. The variation of $\phi_{\max}$ (solid line), the maximum value of ϕ at which there is a switch in the particle magnetic moment, and ϕ_{amp}, the range of variation of ϕ (dashed line) as a function of $\omega^{\dagger}$ for $h_0 = 1.0$ ($\circ$), $h_0 = 0.8$ ($\triangle$), $h_0 = 0.7$ (∇), $h_0 = 0.6$ ($\diamond$). The dotted line on the right has slope -1 on a log-log graph.

The variation of $\phi_{\max}$, the maximum value of ϕ, and ϕ_{amp}, the difference between the maximum and minimum values of ϕ, are shown as a function of $\omega^{\dagger}$ in Fig. 13 for different values of h_0. This figure shows that $\phi_{\max}$ does not vary significantly with $\omega^{\dagger}$, but there is a monotonic decrease in the amplitude of the ϕ variation. For $\omega^{\dagger} \ll 1$, the time period of the magnetic field oscillation is much larger than the particle relaxation time, and the particle orientation responds instantaneously to changes in the field. In this limit, ϕ_{amp} is close to $\phi_{\max}$, indicating that the particle orientation oscillates from $\phi \simeq 0$, the magnetic field direction, to $\phi = \phi_{\max}$. For $\omega^{\dagger} \gg 1$, the time period of the magnetic field oscillation is much smaller than that for orientation relaxation, and consequently there is little change in the particle orientation with change in the magnetic field. Here there is very little variation ϕ with time, and ϕ_{amp} is much smaller than $\phi_{\max}$. The value of ϕ_{amp} decreases proportional to $(\omega^{\dagger})^{-1}$ for $\omega^{\dagger} \gg 1$.

The value of the magnetic field at which there is a switching of the magnetic moment is related to the "switching field" for the Stoner-Wohlfarth model [38] for a stationary particle. The switching field h_s [Eq. (30)] is shown as a function of the angle ϕ for a static particle by the line in Fig. 14. The symbols are the values of $h_0 \cos(\omega^{\dagger} t^{\dagger})$, the instantaneous field at the time instant for switching (dotted vertical lines in Fig. 10), as a function of $\phi_{\max}$, the angle at which the switching takes place. It is evident that when the scaled instantaneous field $h_0 \cos(\omega^{\dagger} t^{\dagger})$ is plotted against the angle $\phi_{\max}$ at which switching takes place, the points fall exactly on the switching field vs angle curve for a static particle. The switching angle has a small variation with $\omega^{\dagger}$ for $h_0 = 0.55$, as shown by the spread in the circle symbols in Fig. 14. As h_0 increases, the dependence of the switching field with $\omega^{\dagger}$ decreases.

C. Transition

A clear distinction has been drawn between the "oscillating magnetic moment" at low h_0, where the magnetic moment executes small amplitude oscillations about one pole of the orientation vector, and the "switching magnetic moment" at high h_0, where the magnetic moment switches between the two poles of the orientation vector which executes small amplitude oscillations about the magnetic field direction. The transition between the oscillating and switching magnetic moment is discontinuous—this is due to the discontinuous change in the moment in Fig. 4. In addition to h_0 and $\omega^{\dagger}$, this transition also depends on the initial orientation angle ϕ_i at $t = 0$. It should be noted

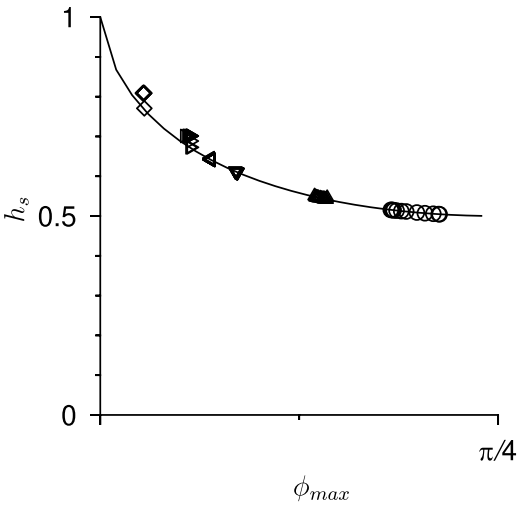

FIG. 14. The switching field h_s [Eq. (30)] as a function of the angle $\phi_{\max}$ between the orientation vector and magnetic field for a static particle (solid line); and the variation of $h_0 \cos(\omega^\dagger t^\dagger)$ with $\phi_{\max}$ for a particle in an oscillating magnetic field, where $\phi_{\max}$ is the angle at which the magnetic moment switches (dashed vertical lines in Figs. 10 and 16). The symbols are $h_0 = 0.55$ ($\circ$), $h_0 = 0.6$ ($\triangle$), $h_0 = 0.7$ (∇), $h_0 = 0.75$ ($\triangleleft$), $h_0 = 0.8$ ($\triangleright$), $h_0 = 1.0$ ($\diamond$).

that ϕ_i is different from ϕ_u shown in Fig. 9; the former is the initial condition, while the latter is the value of ϕ at $\cos(\omega^\dagger t^\dagger) = 1$ for the universal trajectory.

The boundaries between oscillating and switching magnetic moments are shown by the solid lines in the $\omega^\dagger$-ϕ_i plane for $0.55 \leqslant h_0 \leqslant 0.75$. Here ϕ_i is the initial angle of the particle orientation which varies between 0 and $\pi/2$. These boundaries were evaluated numerically at the points shown by circles, where an increment of 0.001 in ϕ_i results in a transition between the oscillating and switching magnetic moment. Also shown in Fig. 15 are the angle ϕ_u (Fig. 9) for periodic states.

(1) If the initial orientation is between two solid lines of the same color, an oscillating magnetic moment is observed where there is a universal trajectory with ϕ_u shown by the dotted line and the $\triangle$ symbol. It is observed that ϕ_u tends to $\pi/2$ for $\omega^\dagger \gg 1$, in agreement with Fig. 9(a).

(2) If the initial orientation is not between the two solid lines, a switching magnetic moment is observed in the long-time limit. The value of ϕ_u [shown in Fig. 9(b) for the switching magnetic moment] is shown by the dashed lines and ∇ symbol in Fig. 15. It is observed that ϕ_u is close to 0, implying that the orientation vector is almost aligned with the magnetic field when the field passes through extrema.

Figures 16(a) and 16(c) show the angles ϕ (black) and $\phi + \alpha$ (blue), and Figs. 16(b) and 16(d) show the angle α at two points on either side of the transition line at the location shown by the black filled circle in Fig. 15. The results for $h_0 = 0.55$, $\omega^\dagger = 1.0$, and $\phi_i = 0.919$ are shown in Figs. 15(a) and 15(b). The parameter values are just below the red boundary at the black filled circle in Fig. 15). The magnetic moment switches, that is, there is a discontinuous change in the orientation of the magnetic moment relative to one pole of the orientation vector, as shown in Fig. 16(a). This is the same as that observed for high h_0 in Sec. V B. The amplitude of the ϕ oscillation in Fig. 16(b) is relatively small, and there is a discontinuity in the slope of the angle ϕ at the instants where the magnetic moment switches. In Figs. 16(c) and 16(d), the trajectories are shown when the initial angle is increased to $\phi_i = 0.920$ while maintaining $h_0 = 0.55$ and $\omega^\dagger = 1.0$. This is just above the red boundary at the black filled circle in Fig. 15. Here it is observed that the magnetic moment oscillates about one pole of the orientation vector, and there is no discontinuous transition. The dynamics is the same as that for an oscillating magnetic moment at low h_0 in Sec. V A.

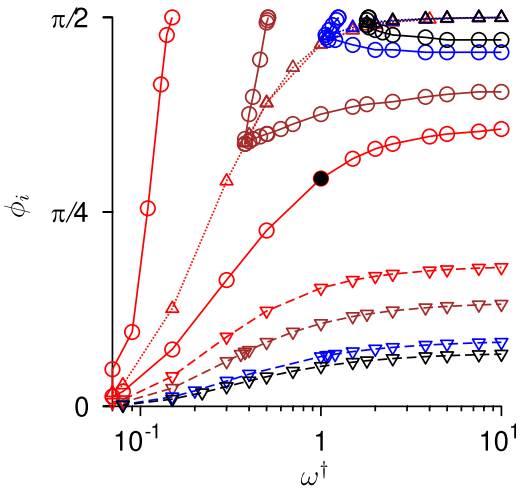

FIG. 15. The solid lines and ○ symbols are the boundaries in the $\omega^{\dagger} - \phi_i$ plane between oscillating and switching magnetic moment at $h_0 = 0.55$ (red), $h_0 = 0.6$ (brown), $h_0 = 0.7$ (blue), and $h_0 = 0.75$ (black). The dotted lines and △ symbol are the values of ϕ_u for the oscillating magnetic moment, similar to Fig. 9(a). The dashed lines and ∇ symbol are the value of ϕ_u [Fig. 9(b)] for the switching magnetic moment, similar to Fig. 9(b). The black filled circle is $\phi_i = 0.920$ at $\omega^{\dagger} = 1$ and $h_0 = 0.55$; Figs. 16(a) and 16(c) show the ϕ variation on either side of the boundary at this location.

For $h_0 \leqslant 0.5$, only an oscillating magnetic moment is observed. At $h_0 = 0.55$, there is a relatively small region outside of the two red lines in Fig. 15, where a switching magnetic moment is observed, while an oscillating magnetic moment is observed between the solid lines. The region between the solid lines shrinks as h_0 is increased, and decreases to zero at $h_0 = 1$, resulting in a switching magnetic moment independent of initial condition.

VI. TORQUE FLUCTUATIONS

The average torque exerted by the particle on the fluid is zero because the particle does not undergo complete rotations. However, there are fluctuations in the torque vector along the perpendicular to the plane of the particle oscillation. The root mean square of the torque fluctuations is shown in Figs. 17(a) and 17(b) for the oscillating and switching magnetic moments, respectively. There is a decrease by an order of magnitude in $T^{\dagger}_{\mathrm{rms}}$ when h_0 is increased from 0.5 to 1.0. Even in the range $0.5 < h_0 < 0.8$, where there is coexistence between oscillating and switching magnetic moments, the torque for the switching moment is significantly smaller than that for the oscillating magnetic moment.

The value of $T^{\dagger}_{\mathrm{rms}}$ does not depend on the initial orientation for the Stoner-Wohlfarth model in Fig. 17. This is in contrast to the root mean square of the torque fluctuations for a permanent dipole in Fig. 6, which does depend on the initial orientation for high $\omega^{\dagger}$. This is because the trajectory of the orientation vector does depend on ϕ_i for a permanent dipole, as shown in Fig. 5(b), but the trajectory for the Stoner-Wohlfarth model drifts to a universal trajectory, as shown in Figs. 8 and 12.

The value of $T^{\dagger}_{\mathrm{rms}}$ for the oscillating magnetic moment is shown in Fig. 17(a). For small h_0, the angle α is $O(h_0)$ [see discussion preceding Eq. (47)], and therefore, the angle between the magnetic moment and the field is approximately ϕ. In this case the trajectory is close to that for a permanent dipole, but with the angle $\phi_i = \pi/2$ in Eqs. (33) and (34). The horizontal dashed line in Fig. 17(a) is the torque predicted by Eq. (43) for $\phi_i = \pi/2$ in the limit $\omega^{\dagger} \gg 1$ [see discussion following Eq. (48)]. For $\omega^{\dagger} \ll 1$, $T^{\dagger}_{\mathrm{rms}}$ increases proportional to $\sqrt{\omega^{\dagger}}$, as predicted by Eq. (42) for $\omega^{\dagger} \ll 1$.

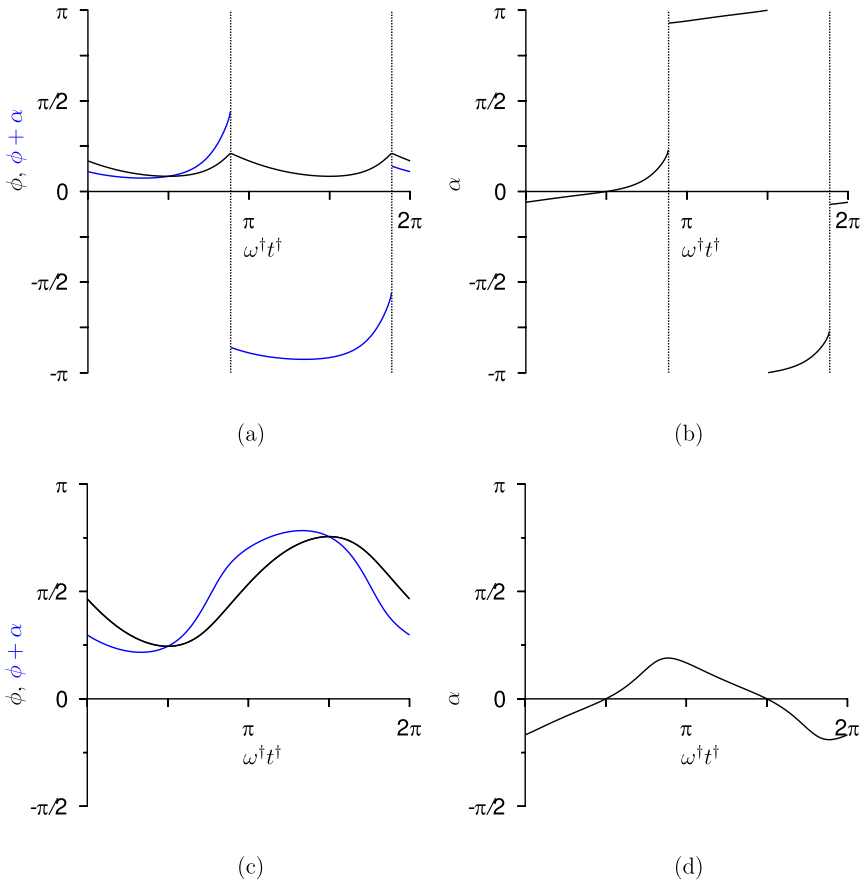

FIG. 16. The angles ϕ of the orientation vector (black), $\phi + \alpha$ of the magnetic moment (blue) (a), (c), and α of the magnetic moment relative to the orientation vector (b), (d), as a function of $\omega^\dagger t^\dagger$ for $h_0 = 0.55$, $\omega^\dagger = 1$ below and above the transition line at the point shown by the black filled circle in Fig. 15 at $\phi_i = 0.919$ (a), (b) and $\phi_i = 0.920$ (c), (d). The magnetic moment switches at the time instants shown by the vertical dotted lines in (a) and (b). Movie 7 [37] compares the dynamics of the particle orientation and magnetic moment for $h_0 = 0.55$, $\omega^\dagger = 1$ and for $\phi_i = 0.919$ (left) and $\phi_i = 0.920$ (right).

The value of $T^\dagger_{\rm rms}$ for the switching magnetic moment is shown in Fig. 17(b). Here the magnitude of the torque fluctuations is much lower than that for the oscillating magnetic moment. For large h_0, the magnetic moment switches between the two poles of the particle orientation axis. The orientation angle ϕ is approximately a constant, $\phi \sim \phi_{\rm max}$ for $\omega^\dagger \gg 1$ (see Fig. 10), and $T^\dagger_{\rm rms}$ can be evaluated assuming a stationary dipole in an oscillating field. The solution for $T^\dagger_{\rm rms}$ is the same as Eq. (43) with $\phi_i = \phi_{\rm max}$, that is, $T^\dagger_{\rm rms} = [\sin(\phi_{\rm max})/\sqrt{2}]$. These solutions, shown by the horizontal dashed lines on the right in Fig. 17(b) are in quantitative agreement with numerical solutions for $\omega^\dagger \gg 1$.

VII. CONCLUSION

The dynamics of a spheroidal magnetic particle in an oscillating magnetic field in the low Reynolds number limit has been analyzed using different models for the particle magnetic moment. There is a steady solution when the particle magnetic moment is aligned along the magnetic field because the torque on the particle is zero in this configuration. Here we examine whether the particle

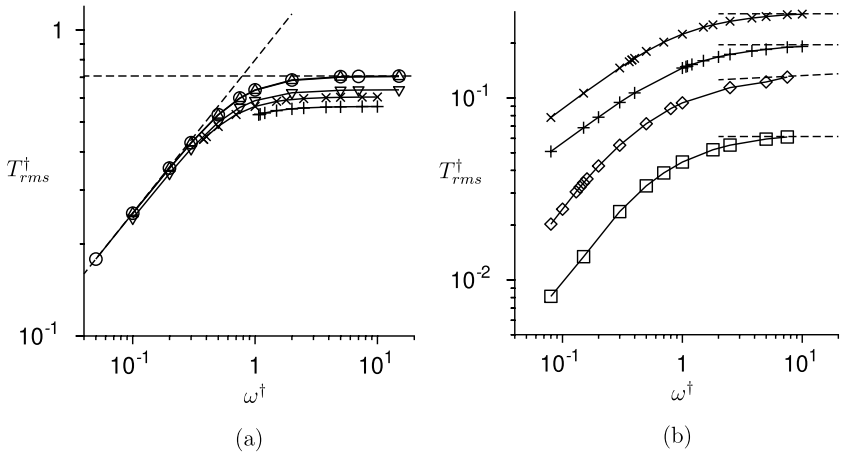

FIG. 17. The root mean square of the torque fluctuations as a function of $\omega^{\dagger}$ for different values of the parameter h_0 in the Stoner-Wohlfarth model, ○—$h_0 = 0.01$, △—$h_0 = 0.1$, ▽—$h_0 = 0.5$, ×—$h_0 = 0.6$, +—$h_0 = 0.7$, ◇—$h_0 = 0.8$, □—$h_0 = 1.0$. Panel (a) is for oscillating magnetic moment and (b) for switching magnetic moment. The sloping dashed line in (a) is $T^{\dagger}_{\rm rms} = \sqrt{2\omega^{\dagger}/\pi}$ [Eq. (42) for $\omega^{\dagger} \ll 1$], and the horizontal dashed line is $T^{\dagger}_{\rm rms} = (1/\sqrt{2})$ [Eq. (43) with $\phi_i = \pi/2$]. The dashed horizontal lines in (b) are $T^{\dagger}_{\rm rms} = [\sin(\phi_{\rm max})/\sqrt{2}]$ [Eq. (43) with $\phi_i = \phi_{\rm max}$].

with an arbitrary initial orientation tends to the stable state, or whether the orientation undergoes oscillations. The root mean square of the torque fluctuations due to particle motion is also examined.

The magnetic moment of the particles is fixed along one of the poles of the orientation vector in the permanent dipole model. In an oscillating magnetic field, a particle with a permanent dipole executes oscillations about its initial orientation. The nature of oscillations depends on $\omega^{\dagger}$, the ratio of the magnetic field frequency and the viscous relaxation rate. There are small amplitude oscillations in the orientation vector about the initial orientation for $\omega^{\dagger} \gg 1$ where the magnetic field frequency is much larger than the viscous relaxation rate. The amplitude of the oscillations decreases proportional to $(\omega^{\dagger})^{-1}$, and the scaled root mean square of the torque fluctuations tends to a constant value dependent on the initial orientation. The time variation of the orientation angle and the root mean square of the torque fluctuations are in agreement with the asymptotic results, Eqs. (40) and (43), in this limit. In the limit $\omega^{\dagger} \ll 1$, where the magnetic field frequency is much smaller than the viscous relaxation rate, and the particle orientation is close to the magnetic field direction for most of the period of oscillation. There are rapid reversals in the orientation when the field passes through extrema. The root mean square of the torque fluctuations (scaled by the characteristic magnetic torque) increases proportional to $\sqrt{\omega^{\dagger}}$ and is independent of the initial orientation, in agreement with Eq. (42) for $\omega^{\dagger} \ll 1$.

For different types of nonhysteretic induced dipole models, considered in Appendix, the orientation tends to a steady orientation along the magnetic field direction. The signum model is a nonhysteretic model where the magnitude of the moment is a constant, and the direction is along the axis of the particle in the direction with a positive magnetic field component. In the linear model, the magnitude of the moment is proportional to the dot product of the orientation vector and the magnetic field, and the direction is along the orientation vector. Analytical solutions are obtained for these two models which show that the particle aligns with the field in the long-time limit. The nonhysteretic Langevin model provides a smooth transition between the linear model for low field and signum model for high field. In this case also, numerical calculations show that the particle aligns with the field direction in the long-time limit independent of the initial orientation.

The Stoner-Wohlfarth is a hysteretic model in which the magnetic moment is not fixed along the particle orientation vector, but there is a free energy penalty due to the angle α between the

particle orientation and magnetic moment. The parameter h_0 is the ratio of the Zeeman energy and the anisotropy energy. Two distinct types of particle motion are observed for the Stoner-Wohlfarth model. For low h_0, the magnetic moment executes small amplitude oscillations about one of the poles of the orientation vector. The dynamics resembles that of a permanent dipole in an oscillating field. The amplitude of the angle α between the magnetic moment and the orientation vector is proportional to h_0 for $h_0 \ll 1$, and the asymptotic results given by Eqs. (47) and (48) accurately capture the difference between the trajectories for the permanent dipole and the Stoner-Wohlfarth model. However, the Stoner-Wohlfarth model is different from a permanent dipole in one important aspect. The trajectory of a permanent dipole depends on the initial orientation. In contrast, the trajectory for the Stoner-Wohlfarth model is independent of the initial orientation in the periodic state in the long-time limit. For arbitrary initial orientation, it is found that the trajectory drifts to a universal trajectory, and the orientation angle tends to a value ϕ_u at $\cos(\omega^\dagger t^\dagger) = 1$. In agreement with the numerical results, an asymptotic calculation shows that $\phi_u = \pi/2 + O(h_0)$ for $h_0 \ll 1$.

For large h_0, the particle orientation executes small amplitude oscillations close to the magnetic field direction, while the magnetic moment switches between directions close to the the two poles of the orientation vector. This is due to the dependence of the anisotropy energy and Zeeman energy on the angle α. The total energy transitions from two minima at two well-separated values of α to one minimum during the sinusoidal oscillation in the magnetic field, and this results in a discontinuous change in the magnetic moment. The discontinuous change in the moment results in a discontinuous change in the torque on the particle and the angular velocity. The amplitude of the particle orientation vector decreases rapidly as h_0 increases. For fixed h_0, the amplitude tends to a constant value for $\omega^\dagger \ll 1$, and decreases proportional to $(\omega^\dagger)^{-1}$ for $\omega^\dagger \gg 1$.

For intermediate values of h_0, there could be an oscillating magnetic moment or a switching magnetic moment depending on the initial orientation angle. The transition between these two types of oscillations is discontinuous as the initial orientation is varied for fixed $\omega^\dagger$.

The nonhysteretic induced dipole models are widely used in literature, whereas real magnetic particles do have some hysteresis, however small. This study demonstrates that for an oscillating field, the result for an induced dipole with hysteresis is qualitatively different from that for a nonhysteretic induced dipole. The latter can not be used as an approximation for the former for an oscillating field, and an accurate model has to at least capture the qualitative features of hysteresis.

ACKNOWLEDGMENT

This work was supported by funding from the MHRD and the Science and Engineering Research Board, Government of India (Grant No. SR/S2/JCB-31/2006) and Synopsys.

There are no conflicts to declare.

APPENDIX: INDUCED DIPOLE WITH NO HYSTERESIS

1. Signum model

The scaled evolution equation for the signum model, Eq. (22), is

$$\frac{d\phi}{dt^\dagger} = -\cos(\omega^\dagger t^\dagger)\sin(\phi)\mathrm{sgn}[\cos(\omega^\dagger t^\dagger)\cos(\phi)]. \tag{A1}$$

Equation (A1) can be written for one cycle of the magnetic field oscillation as

$$\begin{aligned} 0 \leqslant t^\dagger < (\pi/2\omega^\dagger) &: \frac{d\phi}{dt^\dagger} = -\cos(\omega^\dagger t^\dagger)\sin(\phi), \\ (\pi/2\omega^\dagger) \leqslant t^\dagger < (3\pi/2\omega^\dagger) &: \frac{d\phi}{dt^\dagger} = \cos(\omega^\dagger t^\dagger)\sin(\phi), \\ (3\pi/2\omega^\dagger) \leqslant t^\dagger < (2\pi/\omega^\dagger) &: \frac{d\phi}{dt^\dagger} = -\cos(\omega^\dagger t^\dagger)\sin(\phi). \end{aligned} \tag{A2}$$

We have assumed, without loss of generality, that the initial value of ϕ is in the first quadrant. The above equations, (A2), can be solved sequentially using the initial condition $\phi = \phi_i$ at $t^\dagger = 0$ for the first equation, and the final value of ϕ for each equation as the initial condition for the next equation:

$$0 \leqslant t^\dagger < (\pi/2\omega^\dagger) : \tan(\phi/2) = \tan(\phi_i/2)\exp\left(\frac{-\sin(\omega^\dagger t^\dagger)}{\omega^\dagger}\right),$$
$$(\pi/2\omega^\dagger) \leqslant t^\dagger < (3\pi/2\omega^\dagger) : \tan(\phi/2) = \tan(\phi_i/2)\exp\left(\frac{\sin(\omega^\dagger t^\dagger) - 2}{\omega^\dagger}\right),$$
$$(3\pi/2\omega^\dagger) \leqslant t^\dagger < (2\pi/\omega^\dagger) : \tan(\phi/2) = \tan(\phi_i/2)\exp\left(\frac{-\sin(\omega^\dagger t^\dagger) - 4}{\omega^\dagger}\right). \tag{A3}$$

This solution shows that ϕ approaches the fixed point exponentially in time. At $t^\dagger = 0$, the particle starts moving towards the field. This is because the particle moment for the signum model changes sign when the field reverses. This causes the torque on the particle to act in the same direction even when the field reverses. Due to this, the particle orientation angle decreases exponentially in time.

2. Linear model

The scaled evolution equation for the linear model, Eq. (23), is

$$\frac{d\phi}{dt'} = -\cos(\omega' t')^2 \sin(\phi)\cos(\phi), \tag{A4}$$

where the scaled time and frequency are $t' = (t\mu_0\chi H_0^2/A_\perp)$ and $\omega' = (\omega A_\perp/(\mu_0\chi H_0^2))$. For the linear model, there are fixed points at $\phi = 0$ and $\pi/2$. The former is a stable fixed point in which the orientation vector is along the field direction, and the latter is an unstable fixed point where the orientation vector is perpendicular to the field direction. The analytical solution of Eq. (A4) is

$$\tan(\phi) = \tan(\phi_i)\exp\left(-\frac{t'}{2} - \frac{\sin(2\omega' t')}{4\omega'}\right). \tag{A5}$$

Here ϕ_i is the initial value of ϕ at $t' = 0$. Equation (A5) shows that the particle orientation exponentially approaches the field direction. This is because the magnetic moment reverses when the field reverses, and the direction of the torque remains unchanged.

3. Langevin model

The scaled evolution equation for the Langevin model, Eq. (24), is

$$\frac{d\phi}{dt^\dagger} = -\cos(\omega^\dagger t^\dagger)\sin(\phi)\left[\coth\left(\frac{3\chi H_0\cos(\omega^\dagger t^\dagger)\cos(\phi)}{m_0}\right) - \frac{m_0}{3\chi H_0\cos(\omega^\dagger t^\dagger)\cos(\phi)}\right], \tag{A6}$$

where scaled time is $t^\dagger = (t\mu_0 m_0 H_0/A_\perp)$. The two dimensionless parameters in this model are $\omega^\dagger = (\omega A_\perp/(\mu_0 m_0 H_0))$ and $(m_0/\chi H_0)$. The latter is a material-based constant that characterizes the transition from the linear model for low magnetic field to the signum model for high magnetic field.

Equation (A6) is solved numerically, and the results for the variation of the angle ϕ with scaled time are shown in Fig. 18. In all cases, the angle ϕ decreases with time and the particle orientation approaches the magnetic field direction in the long time. For $(m_0/\chi H_0) = 0.001$, the decrease is close to that for the signum model shown by the dotted red lines for the same $\omega^\dagger$. For $(m_0/\chi H_0) = 5$, the decrease resembles that for the linear model shown by the dotted blue lines for the value of $\omega' = \omega^\dagger(m_0/\chi H_0)$, corresponding to the values of $\omega^\dagger$ and $(m_0/\chi H_0)$ for the Langevin model. For an intermediate value of $(m_0/\chi H_0) = 0.8$ and $\omega^\dagger = 0.2$, the linear and signum models decrease

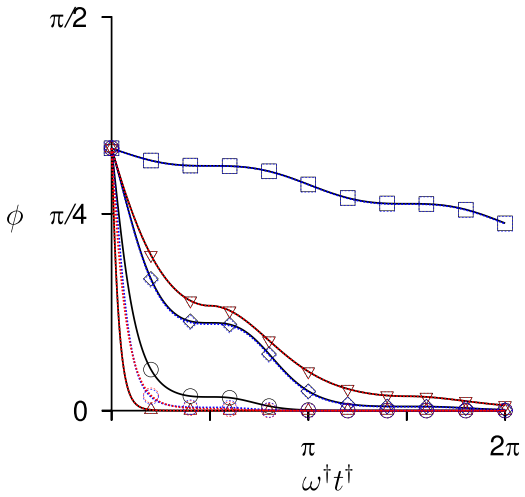

FIG. 18. The variation of the angle ϕ with $\omega^\dagger t^\dagger$ for the Langevin model (black lines) for $(m_0/\chi H_0) = 0.001$, $\omega^\dagger = 0.1$ ($\triangle$); $(m_0/\chi H_0) = 0.001$, $\omega^\dagger = 1$ (∇); $(m_0/\chi H_0) = 0.8$, $\omega^\dagger = 0.2$ ($\circ$); $(m_0/\chi H_0) = 5$, $\omega^\dagger = 0.1$ ($\diamond$); $(m_0/\chi H_0) = 5$, $\omega^\dagger = 1$ ($\square$). The blue dotted lines and symbols are the results for the linear model, $\omega' = \omega^\dagger(m_0/\chi H_0) = 0.16$ ($\circ$),0.5 ($\diamond$) and 5.0 ($\square$). The red dotted lines and symbols are the results for the signum model, $\omega^\dagger = 0.1$ ($\triangle$); 0.2 ($\circ$) and 1 (∇).

faster compared to the Langevin model, but the qualitative nature of the evolution of ϕ is the same. Thus, we find that for nonhysteretic induced dipole models, the angle ϕ tends to a trivial solution where the magnetic moment is aligned along the magnetic field.

[1] E.-S. Shanko, Y. van de Burgt, P. D. Anderson, and J. M. J. den Toonder, Microfluidic magnetic mixing at low reynolds numbers and in stagnant fluids, Micromachines **10**, 731 (2019).
[2] G. Whitesides, The origins and the future of microfluidics, Nature (London) **442**, 368 (2006).
[3] A. deMello, Control and detection of chemical reactions in microfluidic systems, Nature (London) **442**, 394 (2006).
[4] X. Chen and L. Zhang, A review on micromixers actuated with magnetic nanomaterials, Microchim Acta **184**, 3639 (2017).
[5] L.-H. Lu, K. S. Ryu, and C. Liu, A magnetic microstirrer and array for microfluidic mixing, J. Microelectromech. Syst. **11**, 462 (2002).
[6] G. Kitenbergs, K. Erglis, R. Perzynski, and A. Cebers, Magnetic particle mixing with magnetic micro-convection for microfluidics, J. Magn. Magn. Mater. **380**, 227 (2015).
[7] Y. Wang, J. Zhe, B. Chung, and P. Dutta, A rapid magnetic particle driven micromixer, Microfluid Nanofluid **4**, 375 (2008).
[8] M. Kole and S. Khandekar, Engineering applications of ferrofluids: A review, J. Magn. Magn. Mater. **537**, 168222 (2021).
[9] R. E. Rosensweig, Continuum equations for magnetic and dielectric fluids with internal rotations, J. Chem. Phys. **121**, 1228 (2004).
[10] D. W. Condiff and J. S. Dahler, Fluid mechanical aspects of antisymmetric stress, Phys. Fluids **7**, 842 (1964).
[11] A. Chaves, M. Zahn, and C. Rinaldi, Spin-up flow of ferrofluids: Asymptotoic theory and experimental measurements, Phys. Fluids **20**, 053102 (2008).

[12] C. Rinaldi and M. Zahn, Effects of spin viscosity on ferrofluid flow profiles in alternating and rotating magnetic fields, Phys. Fluids **14**, 2847 (2002).
[13] M. Hejazian and N.-T. Nguyen, A rapid magnetofluidic micromixer using diluted ferrofluid, Micromachines **8**, 37 (2017).
[14] C. Y. Wen, C. P. Yeh, C. H. Tsai, and L. M. Fu, Rapid magnetic microfluidic mixer utilizing ac electromagnetic field, Electrophoresis **30**, 4179 (2009).
[15] J. de Vicente, D. J. Klingenberg, and R. Hidalgo-Alvarez, Magnetorheological fluids: A review, Soft Matter **7**, 3701 (2011).
[16] D. J. Klingenberg, Magnetorheology: Applications and challenges, AIChE J. **47**, 246 (2001).
[17] S. G. Sherman, A. C. Becnel, and N. M. Wereley, Relating Mason number to Bingham number in magnetorheological fluids, J. Magn. Magn. Mater. **380**, 98 (2015).
[18] A. V. Anupama, V. Kumaran, and B. Sahoo, Magnetorheological fluids containing rod-shaped lithium-zinc ferrite particles: The steady-state shear response, Soft Matter **14**, 5407 (2018).
[19] V. Kumaran, The effect of inter-particle hydrodynamic and magnetic interactions in a magnetorheological fluid, J. Fluid Mech. **944**, A49 (2022).
[20] Y. Almog and I. Frankel, The motion of axisymmetric dipolar particles in a homogeneous shear flow, J. Fluid Mech. **289**, 243 (1995).
[21] C. A. Sobecki, J. Zhang, Y. Zhang, and C. Wang, Dynamics of paramagnetic and ferromagnetic ellipsoidal particles in shear flow under a uniform magnetic field, Phys. Rev. Fluids **3**, 084201 (2018).
[22] V. Kumaran, Bifurcations in the dynamics of a dipolar spheroid in a shear flow subjected to an external field, Phys. Rev. Fluids **5**, 033701 (2020).
[23] V. Kumaran, Dynamics of polarizable spheroid in a shear flow subjected to a parallel magnetic field, Phys. Rev. Fluids **6**, 043702 (2021).
[24] V. Kumaran, Steady and rotating states of a polarizable spheroid subjected to a magnetic field and a shear flow, Phys. Rev. Fluids **6**, 063701 (2021).
[25] C. P. Moerland, L. J. van IJzendoorn, and M. W. J. Prins, Rotating magnetic particles for lab-on-chip applications—A comprehensive review, Lab Chip **19**, 919 (2019).
[26] G. Helgesen, Propulsion of microspheres in fluids using rotating magnetic fields, Eur. Phys. J. Spec. Top. **227**, 2425 (2019).
[27] P. Fischer and A. Ghosh, Magnetically actuated propulsion at low reynolds numbers: Towards nanoscale control, Nanoscale **3**, 557 (2011).
[28] A. Tokarev, I. Luzinov, J. R. Owens, and K. G. Kornev, Magnetic rotational spectroscopy with nanorods to probe time-dependent rheology of microdroplets, Langmuir **28**, 10064 (2012).
[29] A. Ghosh, P. Mandal, S. Karmakar, and A. Ghosh, Analytical theory and stability analysis of an elongated nanoscale object under external torque, Phys. Chem. Chem. Phys. **15**, 10817 (2013).
[30] C. Kittel, *Introduction to Solid State Physics* (John Wiley & Sons, Hoboken, NJ, 2004).
[31] Q. Li, C. Kartikowati, S. Horie, T. Ogi, T. Iwaki, and K. Okuyama, Correlation between particle size/domain structure and magnetic properties of highly crystalline Fe_3O_4 nanoparticles, Sci. Rep. **7**, 9894 (2017).
[32] W. F. Brown, The fundamental theorem of fine-ferromagnetic-particle theory, J. Appl. Phys. **39**, 993 (1968).
[33] A. Aharoni, Elongated single-domain ferromagnetic particles, J. Appl. Phys. **63**, 5879 (1988).
[34] A. Aharoni, *Introduction to the Theory of Ferromagnetism* (Clarendon Press, Oxford, UK, 1996).
[35] W. F. Brown, Thermal fluctuations of a single-domain particle, Phys. Rev. **130**, 1677 (1963).
[36] G. B. Jeffery, The motion of ellipsoidal particles immersed in a viscous fluid, Proc. R. Soc. Lond. A **102**, 161 (1922).
[37] See Supplemental Material at http://link.aps.org/supplemental/10.1103/PhysRevFluids.9.074303 for the seven movies showing the visual representation of the particle and moment trajectories of a spheroid in the presence of an oscillating field.
[38] C. Tannous and J. Gieraltowski, The Stoner–Wohlfarth model of ferromagnetism, Eur. J. Phys. **29**, 475 (2008).